NEUP Contract no 14-6702

Combining Experiments and Simulations of Extraction Kinetics and Thermodynamics in Advanced Separation Processes for Used Nuclear Fuel

University of California Irvine
Final Report from October 1, 2014 to December 30, 2017

Mikael Nilsson (UCI), Hung Nguyen (UCI), Liem Dang (PNNL), Peter Zalupski (INL), Nathaniel Hoyt (ANL), and Giuseppe Modolo (FZJ)

Intro and Objectives

This 3-year project was a collaboration between University of California Irvine (UC Irvine), Pacific Northwest National Laboratory (PNNL), Idaho National Laboratory (INL), Argonne National Laboratory (ANL) and with an international collaborator at ForschungZentrum Jülich (FZJ). The project was led from UC Irvine under the direction of Profs. Mikael Nilsson and Hung Nguyen. The leads at PNNL, INL, ANL and FZJ were Dr. Liem Dang, Dr. Peter Zalupski, Dr. Nathaniel Hoyt and Dr. Giuseppe Modolo, respectively. Involved in this project at UC Irvine were three full time PhD graduate students, Tro Babikian, Ted Yoo, and Quynh Vo, and one MS student, Alba Font Bosch.

The overall objective of this project was to study how the kinetics and thermodynamics of metal ion extraction can be described by molecular dynamic (MD) simulations and how the simulations can be validated by experimental data. Furthermore, the project includes the applied separation by testing the extraction systems in a single stage annular centrifugal contactor and coupling the experimental data with computational fluid dynamic (CFD) simulations.

Specific objectives of the proposed research were:

1. Study and establish a rigorous connection between MD simulations based on polarizable force fields and extraction thermodynamic and kinetic data.

2. Compare and validate CFD simulations of extraction processes for An/Ln separation using different sizes (and types) of annular centrifugal contactors.

3. Provide a theoretical/simulation and experimental base for scale-up of batch-wise extraction to continuous contactors.

We approached objective 1 and 2 in parallel. For objective 1 we started by studying a well-established extraction system with a relatively simple extraction mechanism, namely tributyl phosphate. What we found was that well optimized simulations can inform experiments and new information on TBP behavior was presented in this project, as well be discussed below. The second objective proved a larger challenge and most of the efforts were devoted to experimental studies.

In the following, each objective will be addressed, what experiments we carried out and our findings. Each objective was addressed although—as will be shown in the report—major challenges were faced in several of the areas studied. Towards the end of the report we also outline outcomes and markers for success from this project.

Objective 1: Study and establish a rigorous connection between MD simulations based on polarizable force fields and extraction thermodynamic and kinetic data.

A major effort of this project was to find parameters for use in MD simulations that would allow us to simulate extraction behavior in various systems. Part of the parameterization procedure require validation of the simulated chemical and physical properties such as dipole moment, density, diffusion coefficient, surface tension etc. Significant effort, more than we had initially anticipated, was spent on careful validation and equipment design to find the needed parameters. The result is that we have fewer data at the end of our project, although we have more confidence in our simulations.

1. Investigations into Tributyl phosphate

As a starting point of this process we used tributyl phosphate as this is a well-studied molecule. Our intentions were to reparametrize this molecule to ensure that the in-silico behavior would match the in-vitro behavior. Our end goal was to provide a consistent set of parameters for TBP, n-dodecane, uranyl, nitrate and water to simulate a 2-phase system. This would allow us to find the energy of the transfer of the uranyl-nitrate-TBP complex from aqueous to organic phase. Using this data, we could find a theoretical mass transfer rate and establish the link to the CFD simulations and kinetic studies described below.

1.1 Force Fields Reparametrization of TBP and n-Dodecane Molecules

Simulations were carried out using the Amber Molecular Dynamics Package. The total interaction potential energy of the Amber force field uses the following Hamiltonian:

$$\mathbf{E_{total}} = \mathbf{E_{bonded}} + \mathbf{E_{nonbonded}} \quad (1)$$

$$\mathbf{E_{bonded}} = \sum_{\mathbf{bonds}} \mathbf{K_r}(\mathbf{r} - \mathbf{r_o})^2 + \sum_{\mathbf{angles}} \mathbf{K_\theta}(\boldsymbol{\theta} - \boldsymbol{\theta_o})^2 + \sum_{\mathbf{dihedrals}}[\sum_{\mathbf{n}} \mathbf{V_n}(\mathbf{1} + \mathbf{cos}(\mathbf{n}\emptyset - \boldsymbol{\gamma_n}))] \quad (2)$$

$$\mathbf{E_{nonbonded}} = \sum_{\mathbf{i<j}} \left[\left(\boldsymbol{\varepsilon_{ij}} \left(\frac{\mathbf{R^*_{ij}}}{\mathbf{r_{ij}}} \right)^{\mathbf{12}} - \mathbf{2}\boldsymbol{\varepsilon_{ij}} \left(\frac{\mathbf{R^*_{ij}}}{\mathbf{r_{ij}}} \right)^{\mathbf{6}} \right) + \left(\frac{\mathbf{q_i q_j}}{\mathbf{r_{ij}}} \right) \right] \quad (3)$$

The terms in order of appearance in E_{bonded} (equation 2) account for bonds, angles, and dihedral angles formation; and in $E_{nonbonded}$ (equation 3) for van der Waals and electrostatic interactions. The specific parameters for each term can be taken from different Amber force fields. R^* is related to σ by the equation: $R^* = 2^{1/6}\sigma$.

Previously, various Amber force fields were primarily developed for proteins and nucleic acid. The general Amber force field (GAFF) was designed in 2004 to include most organic and pharmaceutical molecules.[1] For the GAFF, while the force constants, the parameters of E_{bonded}, and the partial charges of $E_{nonbonded}$ received an overhaul, the LJ parameters were directly taken from older force fields of Amber parm94 and parm99. For this reason, our re-parametrization process focuses on refining the LJ parameters and follows these steps:

1. Initialized MD simulations of bulk liquids using GAFF
2. Calculate density and enthalpy of vaporization of each molecule
3. Compare with experimental values
4. Modify the LJ parameter accordingly

Step 2 to 4 were repeated until the MD and experimental values match. Other properties such as electric dipole moment and self-diffusion coefficient were used as means to validate the refined force fields for TBP and n-dodecane.

Initial results showed good agreement between the experimental and simulated values (Tables 1 and 2).

Table 1. Results comparing different properties of n-Dodecane with experimental values.

	Density (g/cm^3)	ΔH_{vap} (kcal/mol)	Dipole Moment (D)		Surface tension (nM/m)
			gas	liquid	
Non-polarizable	0.744	14.98	NA		20.34
Experimental	0.745	14.70	NA		24.91

Table 2. Results comparing different properties of TBP with experimental values.

	Density (g/cm^3)	ΔH_{vap} (kcal/mol)	Dipole Moment (D)		Surface tension (nM/m)
			gas	liquid	
Non-polarizable	0.971	24.08	3.58		NYD
Experimental	0.973	22.67	3.51		24.9

Using the optimized parameters, we explored different methods, both experimentally and computationally, to study the self-association of TBP at high concentrations of TBP/n-dodecane mixtures.

TBP aggregates larger than dimers were observed in MD simulations as the concentration of TBP increased. The formation of trimers or larger aggregates have been suggested by previous work although the determination of the self-association constants has been a challenge due to the difficulty in measuring the concentrations of various complexes in the solution experimentally. For this reason, an assumption about the insignificant amount of large oligomers has been made; in this case, the equilibrium constants for complexes larger than dimers have been ignored. However, the concentrations of TBP complexes (monomers, dimers and trimers) can be measured directly in MD with the appropriate criteria for what a dimer and trimer is. During this project, we decided to

include both the dimerization and trimerization constants of TBP molecules in n-dodecane solution. We needed a way to identify them in the MD simulations and followed up with an experimental study employing FTIR technique to validate the MD results. The agreement between these studies will be discussed below.

1.2. Potential Mean Force (PMF) of TBP Dimer Conformations

In order to study the self-association of TBP in n-dodecane, we performed a Potential Mean Force (PMF) study using umbrella sampling technique to establish the criteria for identifying TBP dimer and larger aggregates. A 2D PMF study was first carried out along two separate reaction coordinates: distance and angle as depicted in Figure 1. Two TBP monomers were immersed in pure n-dodecane solvent. During equilibration, position constraints were put on the P and O2 atoms so that the monomers were 10.5 Å apart and adapted the antiparallel orientation. During production runs, position restraints were placed on the P and O2 atoms to impose the reaction coordinates. A harmonic force constant of 7 kcal/mol/Å^2 was used for distance restraint and 400 kcal/mol/rad^2 for angle restraint The PMFs were then calculated using the weighted histogram analysis method (WHAM).[2]

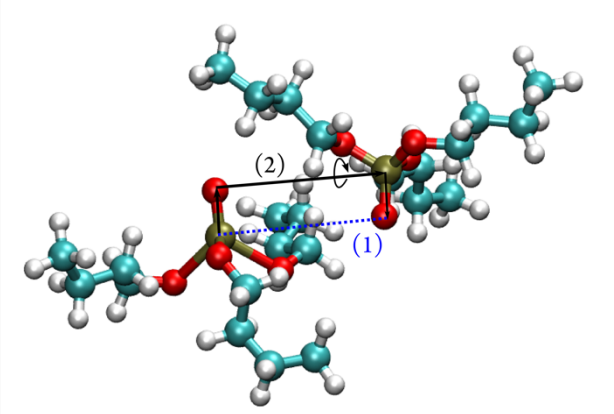

Figure 1. Reaction coordinates for PMF study for two TBP molecules: (1) Distance in Å (2) Angle in degree. Color scheme: red, oxygen atoms; gold, phosphorous atoms; cyan, carbon atoms; and white, hydrogen atoms.

1. The distance (D) between the Phosphorous (P) atom of one TBP molecule to the Oxygen (O2) atom of the other TBP molecule ranging from 3.0 Å to 11.0 Å with an 0.5 Å increment.
2. The pseudo dihedral angle (A) of the two P=O2 double bonds of two separate TBP molecules rotating from 0° to 360° with 5° increment in the curved arrow direction. An angle of 0° or 360° represents the perfect antiparallel orientation whereas 180° represents the perfect parallel orientation.

The contour map of the free energy along reaction coordinates of the pseudo dihedral angles and distances between two TBP molecules is presented in Figure 2A. There is the expected symmetry in the angle reaction coordinate as shown by the blue regions. When two TBP molecules are close to one another (D < 4.0 Å), it is difficult to sample structures in the regions of angles around 100°

~ 300° as demonstrated by the red regions that correspond to high free energy values. They can only assume the anti-parallel orientation due to steric effect, caused by the bulky butyl tails, and possibly the high electrostatic interaction energy of like-sign charges. As they move further away, their free energies minimize but with a clear preference for the anti-parallel (Figure 2B) over the parallel orientation (Figure 2C). The free-energy minima are observed for distances above 4.0 Å with angles in the range of 0° to 60° and 300° to 360°. Specifically, at distances around 5.0 Å - 6.0 Å, the global free-energy minimum is observed over the angle range of 0° - 30°.

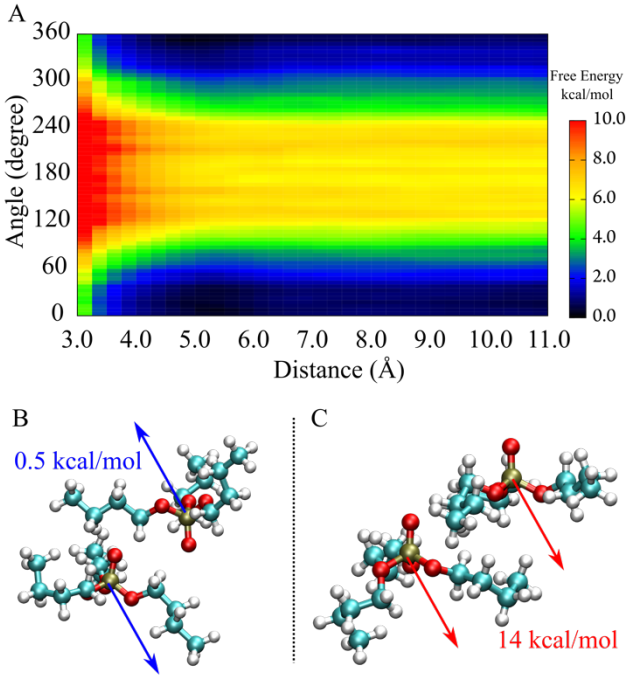

Figure 2. A) The 2D PMF profile along the reaction coordinates distance and angle obtained from umbrella sampling method and WHAM analysis of two TBP molecules; B) Two TBP molecules adopt the anti-parallel orientation and form a stable dimer with low free energy; C) Two TBP molecules assume parallel arrangement and possess high free energy due to steric effect. The arrows represent the direction of each TBP's permanent dipole moment.

The details of the optimization of the non-polarizable parameters and the dimerisation of TBP was published and the work credited to this project. (Vo et al. J. Phys. Chem. B, **119**, 1588−1597, 2015).

1.3. PMF study of TBP trimers and the self-association constants

After the dimer was characterized we continued our efforts to characterize the trimer conformation of TBP. Hence, we expanded upon our previous PMF study of TBP dimer by adding one more TBP molecule to analyze the conformational behaviors of TBP trimers.

The PMF study of TBP trimer was carried out along two different reaction coordinates, distance and angle, as depicted in Figure 3. The P=O bond of the first TBP molecule (designated as TBP1) and the second TBP molecule (TBP2) were held in the perfect anti-parallel orientation and 5.25 Å

apart, representing the TBP dimer based on the results from our study for dimers. The third TBP molecule (TBP3) was added so that the P=O's of TBP2 and TBP3 are also anti-parallel. The distance between TBP2 and TBP3 was varied from 5.0 Å to 7.0 Å with a 0.25 Å increment while TBP3 moves around TBP2 from 60° to 180°. The contour map of the free energy extracted from this examination is presented in Figure 3A. Figure 3B shows one of the most energetically favorable conformations of TBP trimers while Figure 3C presents one of the most energetically unfavorable conformations.

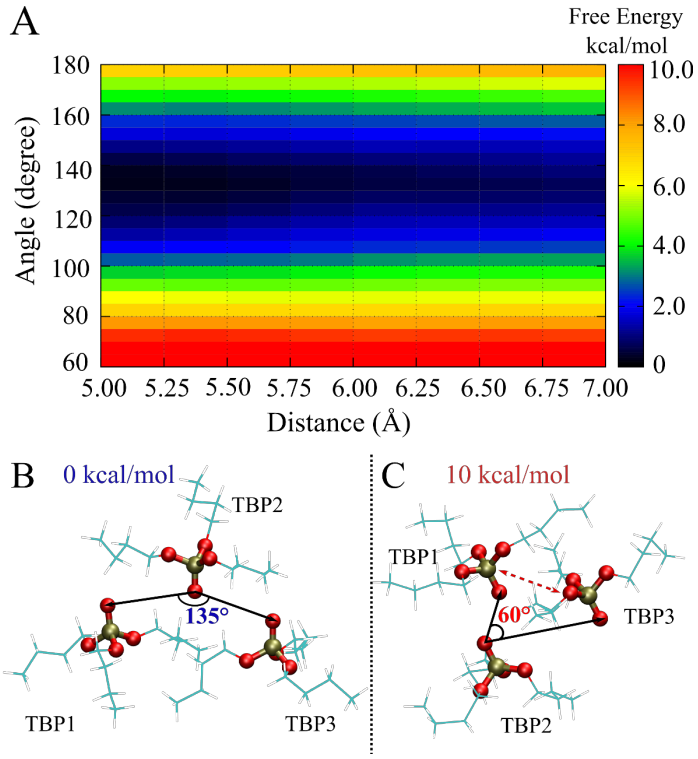

Figure 3. (A) The 2D PMF profile along the reaction coordinates. (B) One of the most energetically favorable TBP trimers conformations. (C) One of the most energetically unfavorable TBP trimers conformations. The butyl tails are shown using line representation for clarity.

The first characteristic of this PMF contour plot is the yellow to red regions, correspond to high free energy, for angles lower than 90° for the full array of the distance reaction coordinate. This is expected since that particular angle range will decrease the separation between TBP3 and TBP1 and also force them to adopt the parallel orientation, which was proven to be highly energetically unfavorable. The angle range of 100° to 160°, in which there is sufficient distance between TBP3 and TBP1, possesses lower free energy indicating the more probable TBP trimer conformations. Another interesting feature obtained from this plot is TBP trimers tend to assume a more angled conformation rather than a linear one. This feature is evidenced by the conformational global free energy minima are around 125°-135° angles while the regions above 160° where all three TBP molecules align yield rather high free energy. The preference for the angled conformation of TBP

trimers can be rationalized by the fact that the polar head groups of TBP are hydrophilic and better shielded from the nonpolar environment of the n-dodecane solvent when they are in this form.

In the next PMF the TBP1 molecule was rotated around its phosphorous atom to vary the pseudo dihedral angle, θ_2, between TBP1 and TBP2 from 0° to 60°. The contour map of the free energy of this second step (Figure 4A) agreed well with our previous calculations. The global free energy minimum is in the TBP1 angle range of 0° to 30° (anti-parallel) and the TBP3 angle range of 125°-135° (angular form) (Figure 4B).

The conformational results from this session agree well with our proposed trimer structure from the RDF calculation. The TBP conformation where its free energy is less than or equal to 3 kcal/mol is used as our criteria to identify TBP trimers. It should be noted that we also used the same free energy threshold for TBP dimers identification.

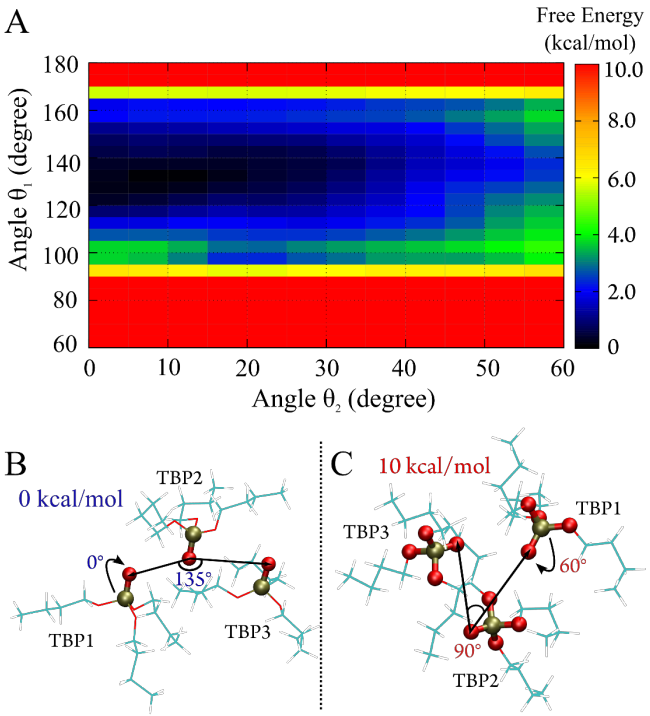

Figure 4. (A) The 2D PMF profile along the reaction coordinates. (B) One of the most energetically favorable TBP trimer conformations. (C) One of the most energetically unfavorable TBP trimer conformations. The butyl tails are shown using line representation for clarity.

1.4. Experimental validation of TBP dimers and trimers.

To validate these simulations, we carried out FTIR studies to experimentally quantify the amount of different TBP aggregates in various TBP/n-dodecane concentrations. FTIR spectra of different TBP concentrations were collected using a super sealed liquid cell. Some representative spectra are shown in Figure 5.

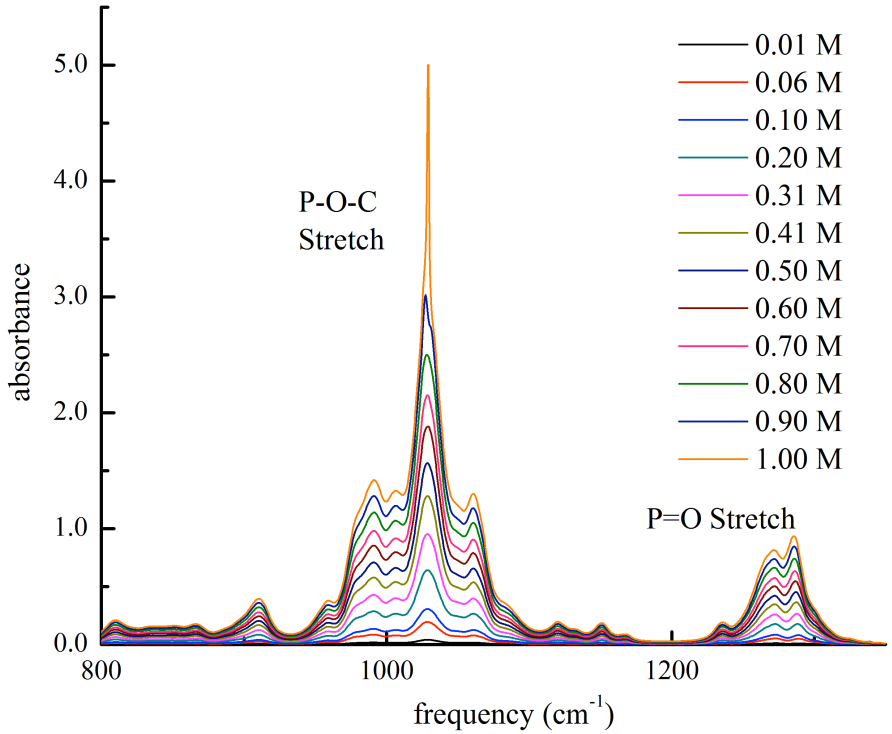

Figure 5. Concentration-dependent FTIR spectra of TBP in n-dodecane solutions. Important spectral regions for the TBP structure are indicated.

We used the Igor Pro program (WaveMetrics, Lake Oswego, OR, USA) to deconvolute the FTIR spectra into a number of Lorentzian functions. The choice of using Lorentzian peak fitting instead of Gaussian or other types is supported by previous FTIR studies. Initially we used only 4 peaks to describe the spectra. These has been initially identified as CH_2 twist, CH_2 bend and the P=O stretchings in two different monomer conformations.[3,4] An example of a spectra at low TBP concentration is shown below in Figure 6. We found that as we increased the concentration of TBP the data was poorly described with only 4 peaks and a 5th peak was introduced and assigned to the dimer. This is also in line with previous investigations.[3,4] As the concentration of TBP increased above 0.3 M a 6th peak was required to provide a reasonable fit to the data, see Figure 7. This final peak was assigned to the trimeric species of TBP. Using the deconvoluted spectra the concentration of each individual species can be found and dimerization and trimerization constants can be calculated. The concentration of each individual species is shown in Figure 8 below.

The criteria extracted from the PMF studies for TBP dimers and trimers were used to identify these complexes in different simulated mixtures with a TBP concentration range from 0.1 M to 1.0 M in n-dodecane. A quick comparison of the mole percentage of each TBP species in the TBP/n-dodecane mixtures between MD study and FTIR data shows excellent agreement (Figure 8). These results give us confidence in our simulations of TBP in n-dodecane under these conditions.

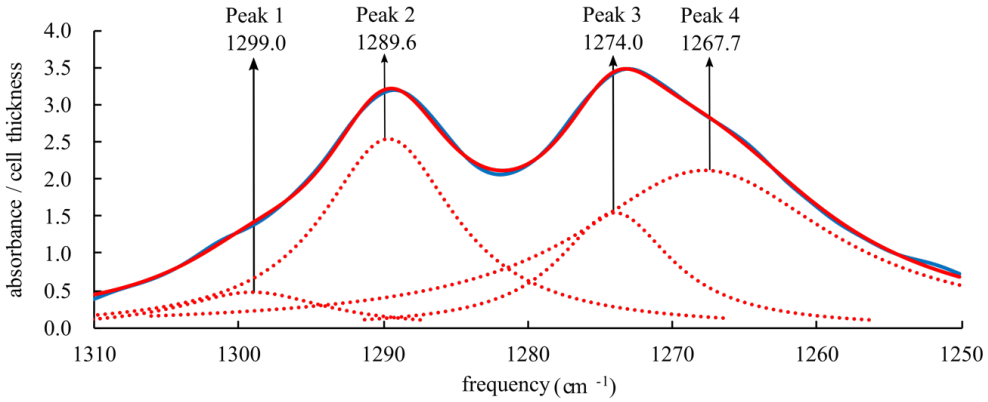

Figure 6. Deconvolution of FTIR spectra at 0.01 M TBP in n-dodecane: red curve: fitted spectrum, blue curve: experimental data, dotted line: four individual resolved peaks. Peak 1: CH_2 twist, Peak 2: P=O stretching in M_2 ('binding' monomer), Peak 3: P=O stretching in M_1 ('non-binding' monomer), Peak 4: CH_2 bend.

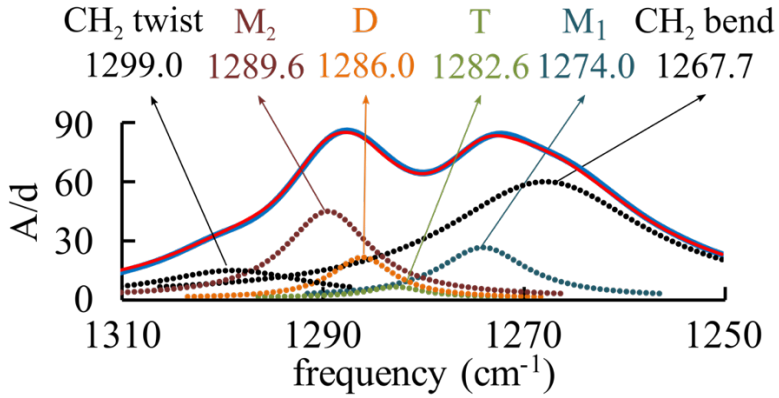

Figure 7. Deconvolution of FTIR spectra at 0.31 M TBP in n-dodecane: red curve: fitted spectrum, blue curve: normalized experiment data, dotted line: five individual resolved peaks. A = absorbance; d = cell thickness.

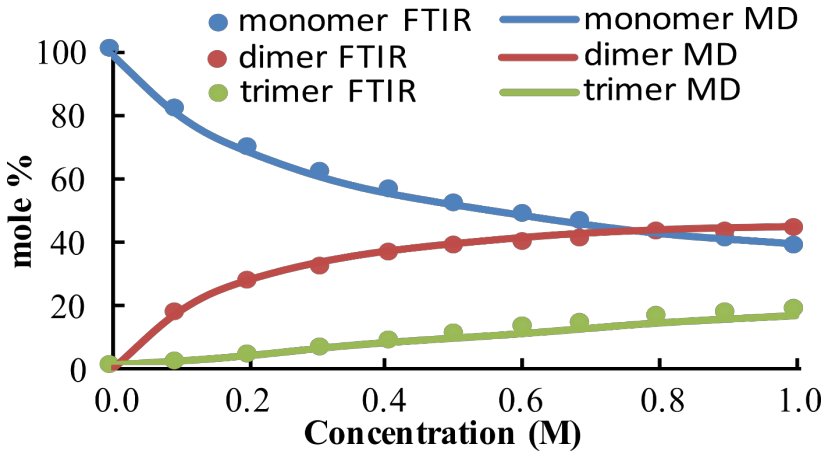

Figure 8. TBP species profile as a function of concentration. Solid lines: results from MD simulations; Circles: results from FTIR data.

The work on the trimerization of TBP was published in two papers in J. Phys. Chem. B. and the work was credited to this project.

1. Quynh N. Vo, Jaclynn L. Unangst, Hung D. Nguyen, and Mikael Nilsson "Quantifying Dimer and Trimer Formation of Tri-n-butyl Phosphates in Different Alkane Diluents: FTIR Study". *J. Phys. Chem. B,* 2016, 120 (28), pp 6976–6984. DOI: 10.1021/acs.jpcb.6b02923

2. Quynh N. Vo, Liem X. Dang, Mikael Nilsson and Hung D. Nguyen "Quantifying Dimer and Trimer Formation of Tri-n-butyl Phosphates in Different Alkane Diluents: Molecular Dynamic Simulation". *J. Phys. Chem. B,* 2016, 120 (28), pp 6985–6994. DOI: 10.1021/acs.jpcb.6b02924

1.5. Polarizable force fields for TBP.

While the behavior of TBP in n-dodecane is well described using non-polarizable force fields, as shown above, for a two-phase system it will be important to include polarizable force fields. During this project effort has been spent on developing polarizable force fields for TBP and n-dodecane molecules. This reparameterization process is more intensive than what is shown above. Specifically, besides adjusting the LJ parameters, ε and σ, of the O2 and P atoms of TBP and of the C atoms of n-dodecane to match the experimental bulk densities and vaporization enthalpies, the atomic partial charges (q) were also scaled simultaneously to reproduce relevant literature values.

The first set of polarizable force field developed for TBP and n-dodecane produced satisfactory agreement with available experimental values for density, heat of vaporization and dipole moment (Table 3).

Table 3. Results comparing different properties of TBP and n-dodecane with experimental values.

	Density (g/cm^3)	ΔH_{vap} (kcal/mol)	Dipole Moment (D) gas	Dipole Moment (D) liquid	Surface tension (mN/m)
TBP	0.970 ± 0.002	23.59 ± 0.02	2.86 ± 1.15	3.33 ± 0.05	26.78 ± 1.10
Exp.	0.973	22.67	3.51 ± 0.23		27.20 ± 0.50
n-dodecane	0.745 ± 0.108	15.49 ± 0.014	0.01 ± 0.001	0.11 ± 0.001	20.86 ± 0.44
Exp.	0.745	14.7	NA		24.9

One of the important parameters for validating polarizable force fields is surface and interfacial tension. Using a Sigma force tensiometer we collected surface (liquid-air) as well as interfacial (liquid-liquid, i.e. organic phase – aqueous phase) tension values. We compared this to simulated values and observed that for surface tension as well as pure n-dodecane or pure TBP our simulations match the experiments (Table 4 and Table 5). In addition to surface tension we also estimated the density profile in each bulk phase and the surface thickness between the two phases.

Table 4. Liquid density, surface thickness and surface tension of TBP in n-dodecane as a function of TBP concentration. Comparison of experimental (Exp) and our simulations (MD).

	Liquid density (g/cm^3)		Surface thickness (Å)	Surface tension (mN/m)	
	MD	Exp.		MD	Exp.
Pure DOD	0.746	0.745	2.88	20.86 ± 0.44	24.98 ± 0.03
0.1 M	0.750	0.756	2.54	21.50	25.09 ± 0.02
0.5 M	0.773	0.762	2.50	21.25	24.87 ± 0.02
1.0 M	0.810	0.806	2.47	22.21	24.88 ± 0.01
Pure TBP	0.962	0.973	3.31	26.78 ± 1.10	27.71 ± 0.04
Pure Water	0.995	0.998	3.20	61.69	72.8

The liquid surface thicknesses listed in table 4 were obtained by fitting the density profile of the liquid into a hyperbolic tangent functional form:

$$\rho(z) = \frac{1}{2}(\rho_L + \rho_V) - \frac{1}{2}(\rho_L - \rho_V)\tanh\left(\frac{z-z_o}{d}\right) \quad (4)$$

In this equation, ρ_L and ρ_V are the liquid and vapor density; z_o is the position of the Gibbs diving surface; and d is the estimated thickness of the interface. Figure 9 shows the calculated TBP and n-dodecane density profiles as a function of the z coordinate normal to the interface average over 10 ns. These density profiles are obtained by computing the liquid densities in slabs of 0.5 Å thickness parallel to the interface.

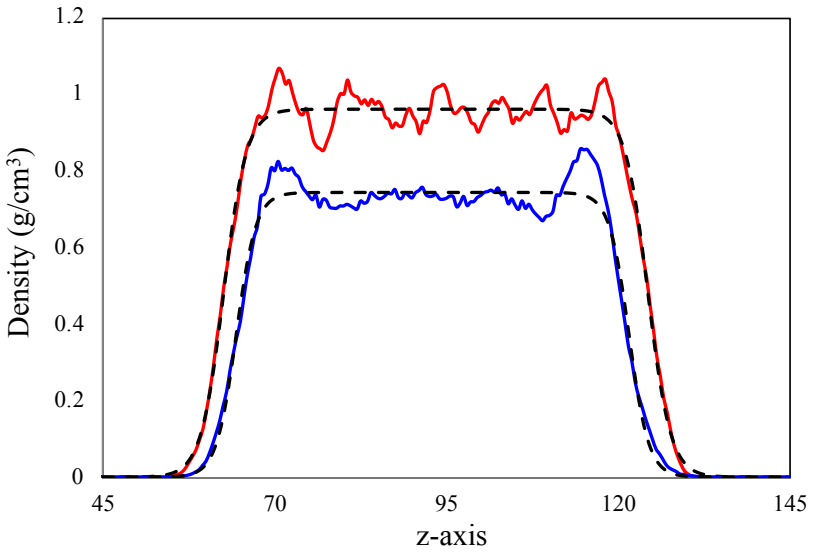

Figure 9. Density profile of TBP and n-dodecane along the z-axis. Red: TBP; blue: n-dodecane; dotted line: hyperbolic fit.

The best fitted curves estimate the bulk liquid densities that match closely with experimental value. From Table 4 it appears that the addition of TBP to n-dodecane up to 1.0 M TBP concentration did not affect the surface tension values in both MD simulations and experiment. The addition of TBP to n-dodecane also seems to have very small effect on the surface thickness. The discrepancies

of the surface tension of the mixtures between simulations and experiments can be attributed to the underestimation of the surface tension of pure n-dodecane and water.

Table 5 shows the results of liquid-liquid interface simulation of TBP/n-dodecane mixtures as a function of TBP concentration. Interestingly, the interfacial thicknesses decrease by roughly 50% in all systems comparing to the surface thicknesses listed in Table 1. The bulk densities of pure n-dodecane and mixtures increase when those systems come in contact with water. This indicated a decrease in the bulk volumes due to the hydrophobicity of n-dodecane. However, in the case of pure TBP and water liquid-liquid interface, the bulk density of TBP decreases while the water interfacial thickness is of the same as its liquid-vapor thickness. These observations suggest that there are interactions between TBP and water at the interface due to the amphiphilicity of TBP.

Table 5. Liquid density, surface thickness and interfacial tension of TBP in n-dodecane as a function of TBP concentration.

	Organic Phase		Aqueous Phase		Interfacial tension (mN/m)	
	Liquid density (g/cm^3)	Interfacial thickness (Å)	Liquid density (g/cm^3)	Interfacial thickness (Å)	MD	Exp.
Pure DOD - WAT	0.810	1.71	0.994	1.67	53.86	50.74 ± 0.08
0.1 M - WAT	0.766	1.28	0.994	1.94	53.0	18.78 ± 0.07
0.5 M - WAT	0.782	1.28	0.994	2.05	49.9	12.24 ± 0.04
1.0 M - WAT	0.799	0.79	0.994	1.92	43.8	10.70 ± 0.02
Pure TBP - WAT	0.958	1.45	0.994	3.13	11.5	7.82 ± 0.28

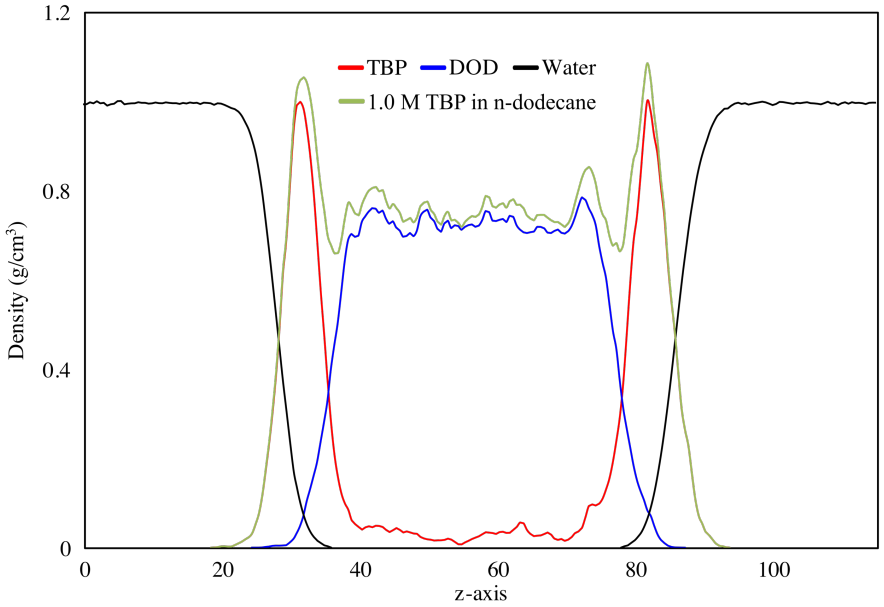

Figure 10. Density profile of 1.0 M TBP in n-dodecane and water along the z-axis of conformation 4 described below.

The density profiles of 1.0 M TBP in n-dodecane and water are shown in Figure 10. It is clear that TBP concentrates at the interface to minimize their potential energy and also dictate the interfacial

area between the two liquids. There are also several TBP molecules distributing within the organic phase instead of migrating to the interfacial. While the trend of decreasing interfacial tension with increasing amount of TBP shown in table 5 is correct, the simulated values for the mixtures show a large discrepancy compared to experimental values. To investigate the reason for this we carried out a number of simulations using different starting conditions.

Configuration 1: Place the two phases in contact after each phase has been pre-equilibrated independently (Figure 11).
Configuration 2: Start with all TBP molecules purposely placed at the interface (Figure 12).
Configuration 3: Start with random configuration of all molecules and let phase separation occur over simulation time (Figure 13).
Configuration 4: Start with all TBP molecules purposely placed at two interfaces (Figure 14).

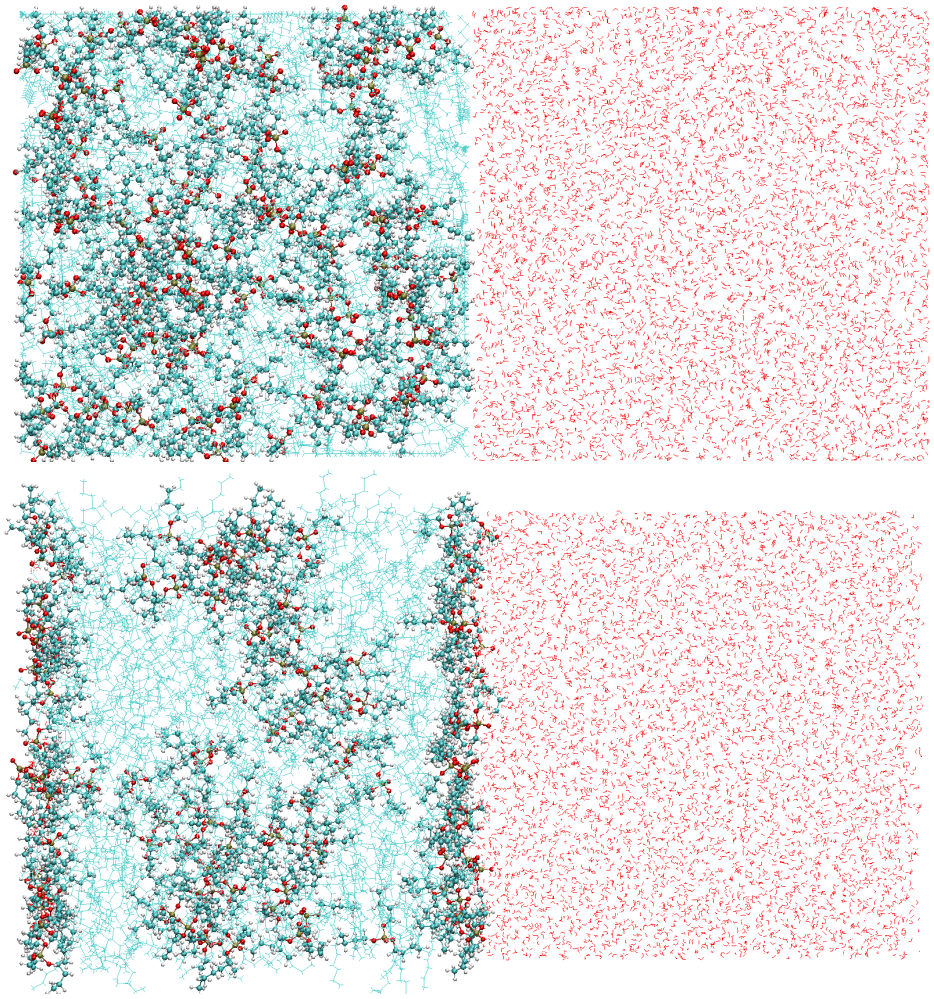

Figure 11: System of separately pre-equilibrated organic and aqueous phases. Red: water molecules; cyan: n-dodecane molecules; CPK presentation: TBP molecules. Top: initial configuration. Bottom: final configuration.

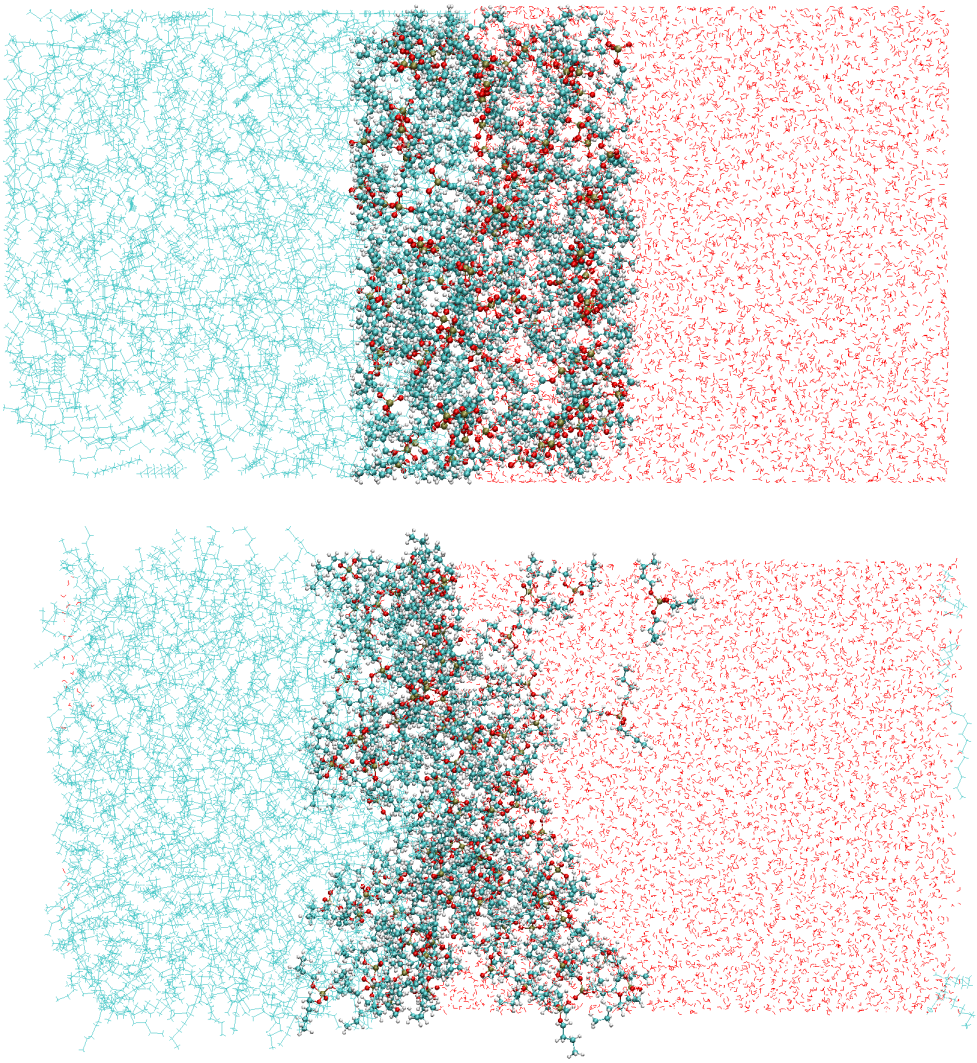

Figure 12: System of TBP molecules placed at one interface. Red: water molecules; cyan: n-dodecane molecules; CPK presentation: TBP molecules. Top: initial configuration. Bottom: final configuration.

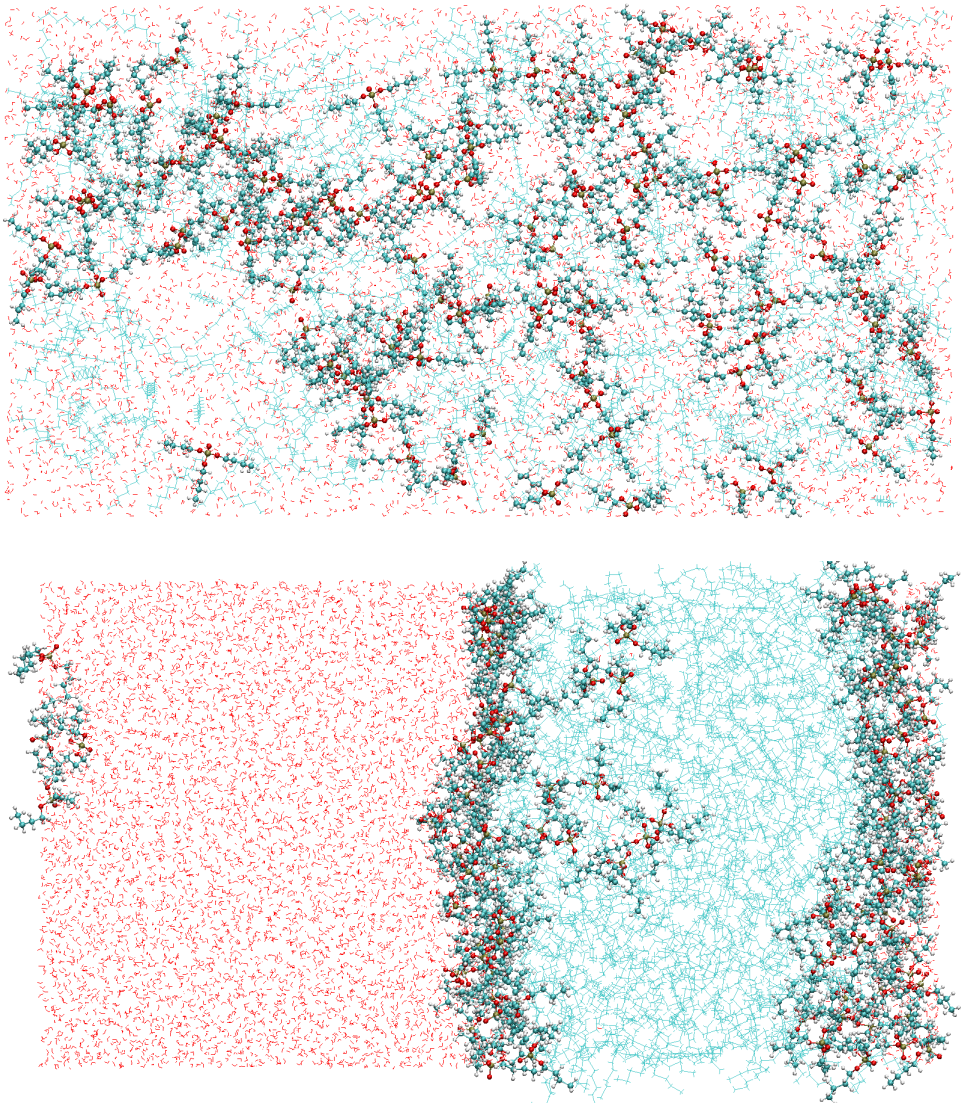

Figure 13: System of mixing TBP, n-dodecane and water randomly. Red: water molecules; cyan: n-dodecane molecules; CPK presentation: TBP molecules. Top: initial configuration. Bottom: final configuration.

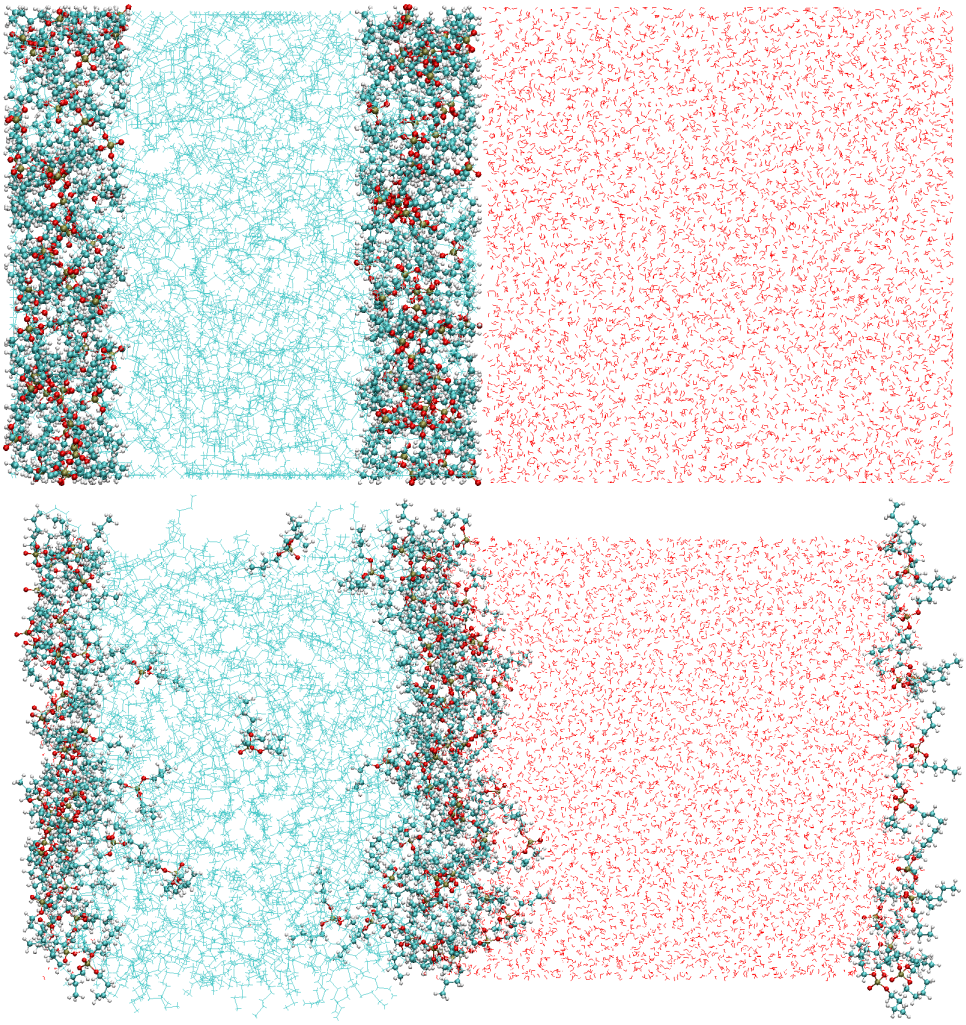

Figure 14: System of TBP molecules placed at two separate interfaces. Red: water molecules; cyan: n-dodecane molecules; CPK presentation: TBP molecules. Top: initial configuration. Bottom: final configuration.

Each configuration was simulated for an extended amount of time in the sense of polarizable force fields. Specifically, conf. 1 and 2 was simulated for 20 ns. Conf. 3 was simulated for 10 ns after phase separation was achieved which took 60 ns. Finally, conf. 4 was simulated for 30 ns. The comparisons of their interfacial tension values are shown in Table 6 below.

Table 6. The effect of the system initial configurations on interfacial tension values

	Interfacial Tension (mN/m) from MD (Experimental value = 10.70)
Configuration 1	43.74
Configuration 2	35.43
Configuration 3	20.73
Configuration 4	19.05

It is obvious from Table 6 that initial configuration has a huge effect on the interfacial tension values of the system. These discrepancies in interfacial tension values due to initial configuration

can be attributed to the equilibration issue that polarizable force fields have to deal with. Ideally, if all initial configurations were run long enough, they would arrive at the same final configuration and produce the same interfacial values. However, computer expenses for these polarizable force field MD simulations are expensive in both computational power and time. For the two configurations that result in an organic phase with most of the TBP molecules in the interface between organic and aqueous phase (configuration 3 and 4) we obtain an interfacial tension value that is closer to the experimental value. For further investigation, the initial configuration in two-phase simulations using polarizable force fields should be based on how the final configuration most likely appears in an experiment.

With these studies, we are reasonably confident that we can simulate the behavior of a two-phase system that includes TBP, n-dodecane and water. The final challenge was to include nitrate ions and uranyl and to simulate the energetics of transferring a TBP-uranyl-nitrate complex from the aqueous phase to an organic phase.

The collaborator at PNNL led efforts to obtain new force fields for the uranyl ion, published in Chem. Phys Letters. In addition, efforts were made to simulate the nitrate ions although the challenge remains on how to validate the chemical behavior of the nitrate ion and thus we cannot report any simulations with confidence. During this project, we initiated simulations of the final complex, shown below in Figure 15. While we are unable to present results in this report we plan on finishing these simulations in the future. Previous studies suggest that the uranyl ions are being extracted in the form $UO_2(NO_3)_2 \cdot 2TBP$ where two TBP bind to UO_2 via monodentate mode and NO_3 via bidentate. The distance between TBP to the U ion is 3 A while it is 2.5 A from the U ion to the two oxygens of the NO_3 molecule. Gas phase simulations are being carried out to verify this structure. Once we can confirm the most favorable conformation for the complex, a PMF study will be performed to study the kinetic of phase transfer of the uranyl complex.

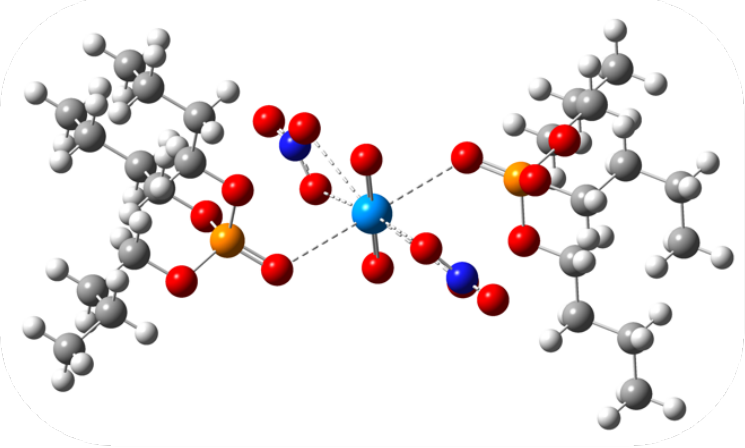

Figure 15. Suggested structure of uranyl complexes in organic phase.

1.6. Summary of TBP studies.

At the end of the project, significant progress has been made on the simulations of the chemical behavior of TBP. We have provided new parameters that well described the behavior in both one and two phases. The two-phase systems require a good initial guess on the final confirmation to allow for a reasonable simulation time. We have shown that a careful simulation can inform

experimental studies as we were able to determine thermodynamic stability constants for the TBP dimer and trimer that agreed well with our simulations. The final goal of simulating the entire complex was unfortunately not reached within the three years of this project. We hope to finalize these studies for the sake of our students' training.

2. Validation and Simulations of Acidic Extraction Systems.

In addition to TBP part of this project was to simulate acidic reagents as they have a great impact on nuclear fuel cycles. We focused our efforts on dibutyl phosphoric acid, HDBP, the main degradation product of TBP. For this reagent, while also relatively well studied, there is significantly less amount of data on the physicochemical properties. One of the key parameters for our validation, the dipole moment, is not reported in the literature. Thus, we spent considerable effort on experimentally determining this variable as described below.

Another main challenge with HDBP is the presence of a –OH group resulting in hydrogen bonding between the molecules. Early on in the project this presented an interesting observation where large aggregates of HDBP molecules appeared to form via hydrogen bonding network. As there is no experimental evidence for this behavior we had to carefully evaluate our simulations so that we do not overestimate the strength of the hydrogen bond resulting in large aggregates.

2.1. Determination of the dipole moment of HDBP

During this project we constructed, tested and validated an instrument that will measure dipole moments of solutions of extracting reagents in dissolved in non-polar solvents. This would allow us to expand the number of substances used for benchmarking our simulations.

To measure dipole moments, we utilized the procedure described in a paper by Janini and Katrib. [5] In their paper, they cite Guggenheim's formulation of the Debye-Onsager equation that simplifies the measurement of dipole moments for polar substances. Guggenheim shows the relationship between dielectric constant, index of refraction, and the concentration of a polar solute in a non-polar solvent at low concentrations. The result is as follows.

$$\frac{\varepsilon-1}{\varepsilon-2}-\frac{\eta^2-1}{\eta^2-2}=\frac{4\pi N_a\mu^2}{9kT}l \qquad (5)$$

Where ε is the solution dielectric constant, η is the index of refraction of the solution, μ is the dipole moment of the pure polar substance of interest, and l is the concentration. By measuring the dielectric constant and index of refraction as a function of concentration, we can calculate out the dipole moment from the slope.

Index of refraction was measured from a refractometer. A simply way to measure the dielectric constant of a material is to measure its capacitance. For this end, we developed the setup shown in Figure 16. The device is based on a conductivity probe and though there are commercially available dipolometers our probe is far less expensive.

Figure 16. Measurement cell and capacitance bridge

The liquid capacitance cell is made from three concentric steel tubes separated by a PEEK spacer. In addition to holding the liquid, the tubes act as electrodes. The two tubes that make the base are welded together and electrically connected. The third tube slides between the two that make the base, creating a cylindrical capacitor. The relationship between capacitance and dielectric constant is:

$$\varepsilon = \frac{C}{C_0} \qquad (6)$$

Where C_0 is the capacitance of the dry cell.

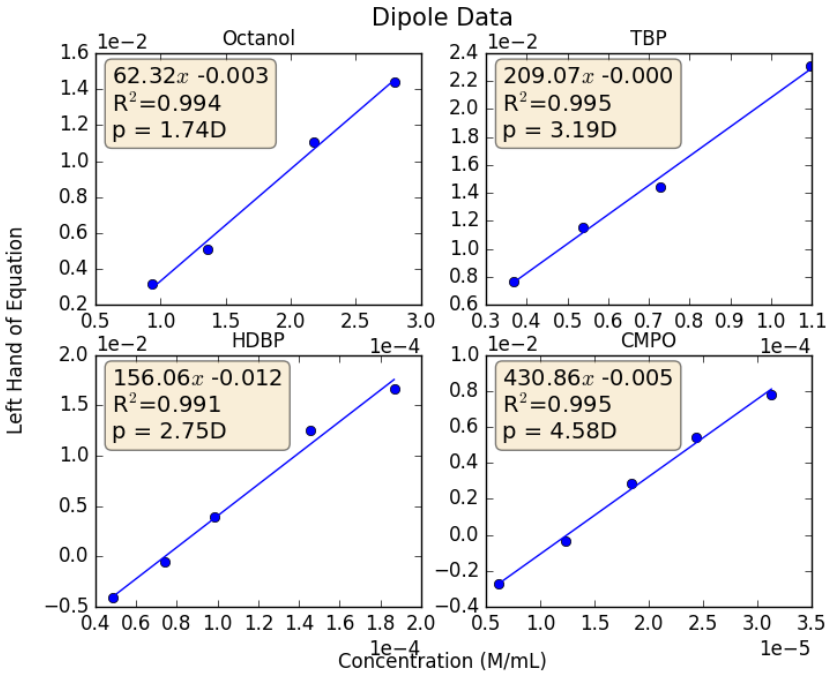

Figure 17. Left hand side of equation 1 plotted versus the concentration of solute using heptanes as the solvent. The dipole moment may be calculated from the slope.

Figure 17 above show the results from measurements using the capacitance cell. 4 different substances were tested, 3 extracting reagents and one polar solvent, diluted in heptane. Octanol

and TBP were used to validate our setup as previous values of the dipole moment exist in the open literature. HDBP and CMPO were tested so that we may find the dipole moment needed to match the MD simulations during the parameterization phase. In addition to the experimental values we used Gaussian to perform quantum mechanical computations to predict dipole moments. The values are shown in Table 7 below. Overall the experimental values for octanol and TBP match well with literature values providing confidence in our method. The experimental dipole moment of HDBP was established and we also show that QM calculations may be used for a rough prediction of the dipole moment of different substances.

Table 7. Comparison of literature and estimated dipole moments for TBP and Octanol. The experimentally determined dipole moments for HDBP and CMPO are shown as well. The diploe moments estimated by QM calculations (Gaussian09) are shown for comparison.

μ (D)	Literature	Gaussian09	Experiment
Octanol	1.74	NA	1.74
TBP	3.35 ± 0.23	3.39	3.19
HDBP	NA	2.70	2.75
CMPO	NA	6.82	4.58

The work on developing the liquid capacitance cell and the determination of the dipole moment of HDBP was written up in a manuscript that was recently (at the time of writing) accepted in the Journal of Solution Chemistry (Yoo et al., J. Sol. Chem., 2018).

2.2. HDBP simulations.

The HDBP molecule was parameterized as previously described for TBP and we attempted to match the density, heat of vaporization and dipole moment with experimental values.

Since there are no reported values for heat of vaporization of HDBP we applied the method of determining heat of vaporization via the Hansen-Beerbower method. Using this method provided a heat of vaporization that matched experimental values of TBP and HDEHP providing some confidence that a value for HDBP may be acceptable. The value found for HDBP was 17.5 kcal/mol and using this as our 'target' value we have successfully parametrized the force field of HDBP, shown in table 8.

Table 8. Values of validation properties for HDBP. Experimental value for heat of vaporization was based on calculations using the Hansen-Beerbower method. The density and dipole moment was determined experimentally in our laboratory.

	Density (g/mL)	ΔH_{vap} (kcal/mol)	Dipole Moment (D)
Experiment	1.06	17.5	2.75 +/- 0.07
Parametrized Model	1.06 +/- 0.005	18.22 +/- 0.45	2.72 +/- 0.02
Difference (%)	0.00	3.81	1.20

To find the conformation of the HDBP dimer we carried out PMF calculations for a number of different conformations. In our case, we generated two sets of two-dimensional PMFs of the HDBP dimer. The first PMF varies the distance between the two phosphorus atoms (PP) and the pseduo-dihedral angle made with P=O bonds (OPPO) along the PP distance vector.

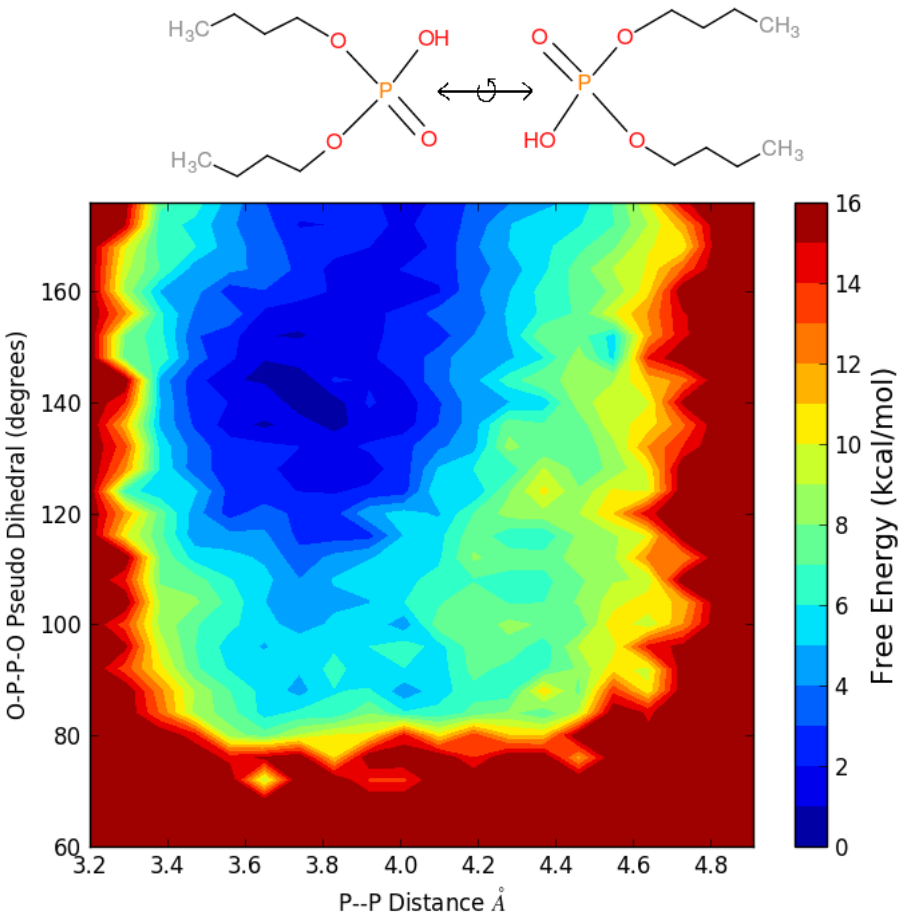

Figure 18. PMF of the O=P – P=O pseudo-dihedral angle vs P to P distance.

Each of these PMFs were carried out to answer a different question. The first PMF, shown in Figure 18, tells us about the conformation of the HDBP dimer. We see that the PP distances that fall within the lowest 1 kcal of free energy is around 3.6 Angstroms. This corresponds to a hydrogen bond donor-acceptor distance of around 2.8 Angstroms. The value is close to existing density function theory calculation for HDEHP done by Luo et al.[6] Their study states that HDEHP has a donor-acceptor distance of 2.6 Angstroms. Given that the only difference between HDEHP and HDBP lies in their alkyl chains, we believe that this value is appropriate for HDBP as well.

From Figure 18 it can be seen that the pseudo-dihedral angle for the lowest energy conformation is not 180 degrees, as what would be expected for a perfect head-to-tail cyclic dimer. Rather, the optimal angle is offset at by around 40 degrees. In addition, there is a large degree of conformal freedom. This is evidenced by the wide range of angles that spans the 0-3 kcal range, which is a range that a molecule can easily explore.

In regards to donor-acceptor distance a second PMF was carried out. This PMF was designed to provide the energy penalty involved in removing a hydrogen bond from an HDBP aggregate. Most studies on phosphoric acid reagents suggest that in non-polar solvents they exist as a dimer. To create a larger aggregate the dimer need to open up allowing for a third HDBP molecule to coordinate, and so on. From our simulations, we cannot rule out higher order aggregates, thus it will be good to know what sort of energy penalty must be paid to make such aggregates, i.e. breaking the hydrogen bonds in a HDBP dimer. The results of our PMF study, shown in Figure 19, indicate that as the molecule is rotated so that one of the hydrogen bonds is broken there is a significant increase in the free energy. This is not unexpected and suggest that the dimer is relatively stable in non-polar solvents, as suggested by previous literature.

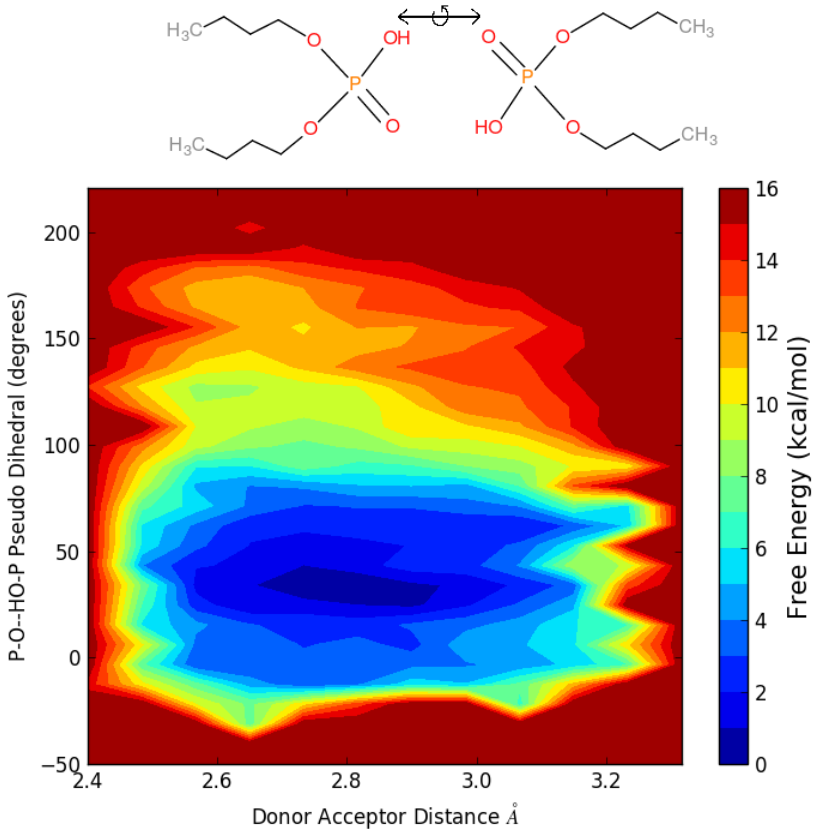

Figure 19. PMF of the P-OH – O=P pseudo-dihedral angle vs donor acceptor distance.

2.3. Summary of HDBP studies.

At the end of the project, we can provide optimized force fields for HDBP for non-polarizable MD simulations. While these have some use in a single-phase simulation the two-phase simulation would require expanding to polarizable force fields. Furthermore, there is a significant challenge in that the proton on HDBP is labile and during complexation or at elevated pH the proton will be lost. This cannot be simulated using the MD approach we have presented here and reactive force fields must be included, making the simulations very expensive. Nevertheless, our efforts provide a starting point to future work. In addition, we have developed

the capability to generate experimental values for the dipole moment for existing as well as future extracting reagents.

Objective 2. Compare and validate CFD simulations of extraction processes for An/Ln separation using different sizes (and types) of annular centrifugal contactors.

For this objective we would compare results from metal ion extraction using annular centrifugal contactors. During this project 5 different contactors were tested for the extraction of dysprosium using Cyanex 923. The distribution ratios of dysprosium as well as hydrodynamics of the contactors were studied. The plan was to simulate these contactors using computational fluid dynamics, specifically the OpenFOAM package. The simulation aspect of this project appeared to be a challenge and a majority of the effort was spent on gathering experimental data. In addition, some of the validation studies required careful kinetic studies and significant time was spent setting up a kinetics cell as described below. At the end of this project this objective fell short although there are several studies in the work, described below, that we intend to finalize and disseminate in journal articles crediting this project.

3. Experimental Studies on Extraction Kinetics and Mass Transfer

3.1. Extraction studies with 1.2 cm annular centrifugal contactor.

The first set of experiments were carried out to compare metal ion distribution between batch and contactors. Dysprosium was chosen for extraction and the concentration in organic and aqueous phase after contact was analyzed using neutron activation. The large neutron capture cross section of dysprosium makes it a good choice for this study since it allows the preparation of dilute systems that are easily analyzed. The organic phase contained IsoparL as the diluent and Cyanex 572, an acidic phosphorus based chelating extractant (Cytec), as the extractant.

The annular centrifugal contactors used was a 5cm CINC contactor (model VO2) and a 1.2cm Robatel (BX012) contactor, Figure 20. The CINC contactor was initially connected to peristaltic pumps that did not provide a stable flow rate. We replaced the pumps with more efficient positive displacement pumps and were able to collect representative data. The Robatel contactor was connected to syringe pumps providing a stable flow rate to the contactor. For the batch extraction experiments equal volumes of organic and aqueous phase were contacted using a vortex mixer.

Figure 20. Left, Robatel BXP012 contactor with syringe pump. Middle, rotor. Right, Stationary housing.

The results are shown in Figure 21. In the study the flow rate was varied, effectively changing the residence time in the contactors. The O/A ratio in the contactor was kept at 1. In the figure, "recycled organic" indicate that the organic solution was used in a previous experiment and was washed between studies; "High to Low" and "Low to High" indicate that the flow rate started high and was lowered, and vise versa. Our study on the extraction efficiency of dysprosium in CINC V02 centrifugal contactors showed that maximum efficiency did not occur at the lowest flow rate (highest residence time) applied as seen in Figure 21. The data for the Robatel contactor is in line with expectations and the extraction is increasing with increased residence time.

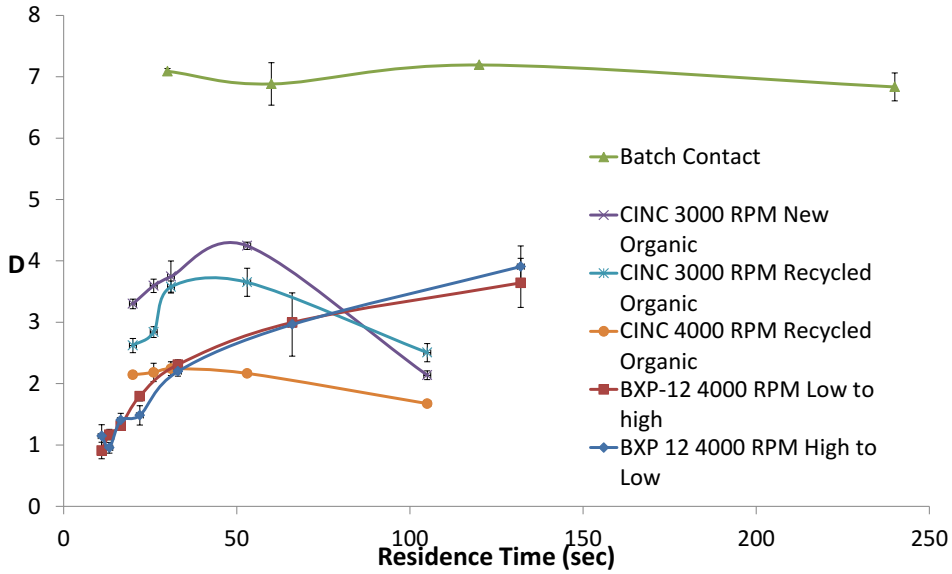

Figure 21. Extraction of dysprosium by 0.2 M Cyanex-572 in IsoparL as a function of residence time in a centrifugal contactor. The batch extraction data is a function of contact time on a vortex mixer. The aqueous phase contained 0.1 mM Dy(III) in 0.1 M HNO_3.

From Figure 21 it is apparent that the extraction efficiency in the Robatel BXP012 centrifugal contactor was less compared to batch extraction experiments conducted under similar conditions. To address the issue, it was necessary to determine the holdup volume of the centrifugal contactor. We observed that the collector rings in the contactor contributed significantly to the total volume of fluid in the contactor indicating that simple measurements of the mass or volume of the fluid collected by draining the contactor would not be an accurate representation of the holdup volume. The approach selected in determining the holdup volume was through measuring the holdup time in the contactor by residence time distribution experiments.

The experiments for residence time were carried out by contacting an aqueous phase, containing a measurable tracer, with an organic phase that would be inert towards the tracer. The inert solute is added as a pulse and tracking the time it would take for the total amount of injected trace solute to clear the contactor would provide a number of the residence time. For the aqueous phase, dysprosium nitrate was used as the tracer and the concentration of the outlet stream was measured by neutron activation analysis. The results summarized in Figure 22 and Table 9.

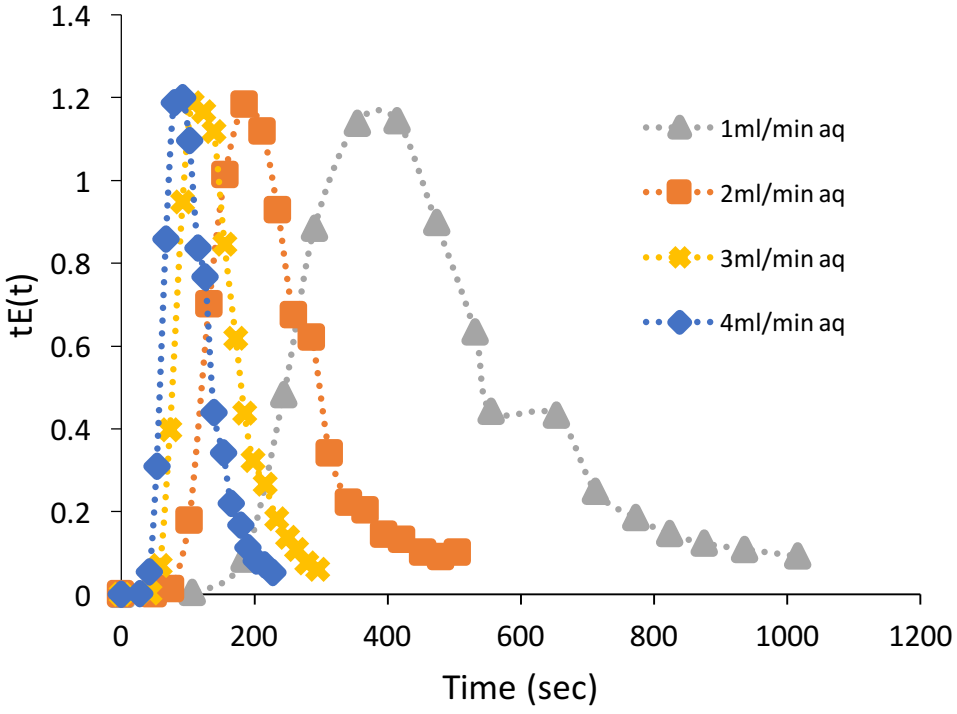

Figure 22. 4000 RPM aqueous continuous consisting of 0.1M HNO_3 in contact with clean IsoparL at O/A=1

Figure 22 shows a function E(t), which is the probability per unit time that the tracer would exit the contactor. This is multiplied with time to get t*E(t) which when integrated over time from t=0 to t=infinity would provide the residence time of the trace dysprosium. The huge difference

between the residence times at different flow rates, which is calculated based on the reactor volume reported by Robatel, and the average holdup time, which is the experimental RTD value, is attributed to the relatively large collection ring in the contactor where no extraction occurs. Table 9 also show a comparison between the apparent residence time calculated by taking the ratio of the reported internal volume of the contactor and the volumetric flow rate. Overall the measured residence times from the RTD experiments differ by 16-17%.

Table 9. Summary of the results from the aqueous RTD experiments at 4000 RPM in the BXP012 contactor.

FlowRate (ml/min)	Residence Time (sec)	Mass Balance	Average Holdup Time (sec)	% Match with Apparent Residence Time
1	66	0.999	412.1	16
2	33	0.997	204.6	16
3	22	0.999	126.6	17
4	16.5	0.999	95.4	17

The organic phase holdup time was also studied by residence time distribution experiments. As before, an inert tracer was added as a pulse and we tracked the time it would take for the total amount of injected trace solute to clear the contactor. For these experiments the inert tracer was a Cyanex 923 – dysprosium complex and the conditions in the aqueous phase were such that there was negligible back-extraction. The aqueous phase consisted of 3 M ammonium nitrate at elevated pH and the dysprosium back-extracted was checked by sampling the aqueous phase. Figure 23 below show how the residence time for both the aqueous and organic phase varies with flow rates for different stirring speeds.

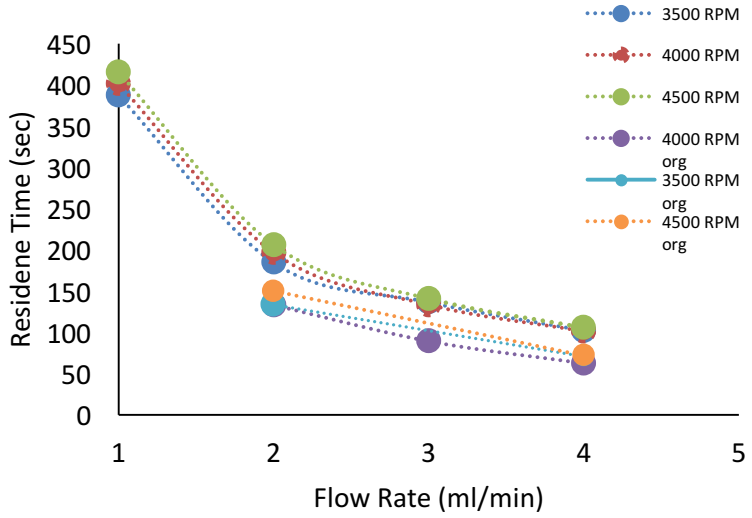

Figure 23. Average residence time of tracer in the Robatel BXP012 as a function of flowrate at varying rotor rotation speed and for the different phases.

From these observations, we can see that the residence time decreases with increasing flowrate, as expected, given that we do not have any accumulation of liquid in the system. We also observe that for the BXP012 contactor the rotor mixing speed have negligible effect on the residence time in both the aqueous and organic phase.

The effect of rotor spinning speed on extraction was also studied. The results are summarized in Figure 24.

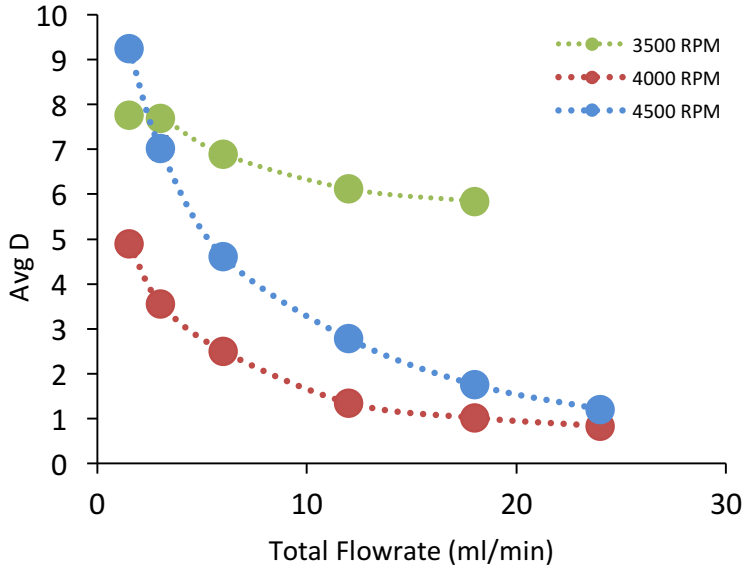

Figure 24. Average distribution ratio of 0.1mM $Dy(NO_3)_3$ with 0.2M C572 as a function of flow rate at varying RPM and with aq/org ratio of 2.

We can see from Figure 24 that as the flowrate increases the distribution ratios decrease due to the decrease in holdup time, and hence decrease in contact time. Using a rotor speed below 3500 rpm result in phase contamination where the organic phase exits together with the aqueous phase in the heavy outlet. Also, using a rotor speed above 4500 rpm results in aqueous phase appearing with the organic phase in the light outlet. The reason for the lower extraction at higher stirring speed is not clear but one possible explanation is that the rotor start to 'slip' and lose grip on the liquid at high speeds resulting in larger droplets and less mass transfer. It is also worth noting that the Robatel contactor is less reproducible compared to other contactors used in this project.

To further investigate the behavior of the solution in the mixing zone of the contactor, we replaced the metal housing with a 3D printed PMMA housing. With the clear housing, the height of the fluid column in the mixing zone was imaged during the RTD experiments. As shown in Figure 25, at 3500 RPM there is minimum volume of fluid in the mixing zone and it increases with increasing RPM. Past around 5000 RPM, the mixture in the mixing zone starts to spill over into the organic collector ring, flooding the contactor. The point at which flooding happens is however also dependent on the flowrate of the phases. It was observed that increasing the flowrate could help in preventing this flooding behavior as RPM increases.

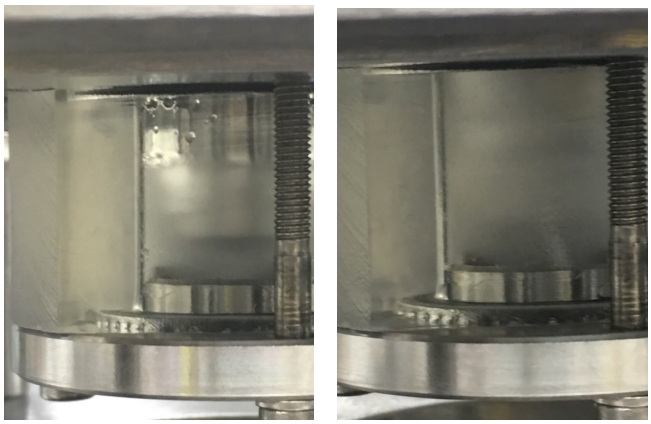

Figure 25. Height of fluid column in the mixing zone at 3500 RPM left and 4500 RPM right.

Although the height of the fluid changes in the mixing zone as seen in Figure 25, this change may not be significant enough to be reflected in the averaged value obtained by the RTD experiments. Also, lower holdup volume in the mixing at 3500 RPM compared to 4500 RPM does not explain the enhanced extraction at the former condition.

While we are able to observe total residence time in the contactor the time in the mixing zone vs the phase separation zone is unknown. To gauge this, we needed to have an idea of the mass transfer kinetics of the dysprosium in this system. Assuming that the dysprosium is transferred between the phases when the phases are well mixed would allow us to estimate the time in the mixing zone. In addition, the mass transfer kinetics was important for the CFD simulations as described below. To find the kinetics of mass transfer a stirred cell was used as described below.

Overall the miniature centrifugal contactor behaved as expected in terms of the total hold-up time. We observed, using the clear housing, that the Robatel contactor has some hydrodynamic instabilities. To successfully interpret the metal extraction trends additional data on the kinetics and hydrodynamics are needed which we were hoping to gain from experiments with the stirred cell and the CFD simulations, respectively.

3.2. Experimental studies using custom made contactors.

In addition to the Robatel contactor, three 3D printed contactors from Argonne National Laboratory were tested. The rotor diameter is 2 cm in two of these contactors and the third contactor has a rotor diameter of 1 cm. Furthermore, one of the 2 cm contactors have a housing that is designed for extended contact time in the mixing zone, figure 26.

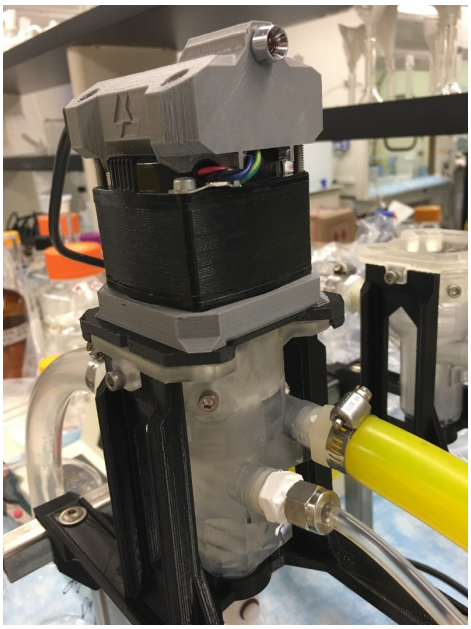

Figure 26. 3-D printed centrifugal contactor with 2 cm rotor. The model shown here has an extended mixing zone and the model in the background (right side in the figure) has the standard mixing zone.

We performed a comparative study with the three ANL contactors and the Robatel BXP012 contactor. In this study, 0.1 mM $Dy(NO_3)_3$ in 0.1 M NO_3 was extracted into the organic phase consisting of Isopar L and 0.2 M C572. Large batches of both solutions were prepared to ensure consistency between all experiments. The rotor speed on the ANL contactors is fixed at 3600 RPM therefore the same RPM was chosen for the Robatel contactor. In all experiments, both pumps were started together and the time for both phases to start exiting the contactor was noted. Before collecting the first sample from both exits we waited an equivalent amount of time to ensure hydrodynamic stability in the contactor. For each experimental condition, i.e. flow rate and flow rate ratio, triplicate samples were collected at different times during the experiment. In both sets of experiments the total flow rate of phases was kept constant. Figures 27 and 28 show the results obtained using a org:aq flow rate ratio of 1:1 and 2:1, respectively.

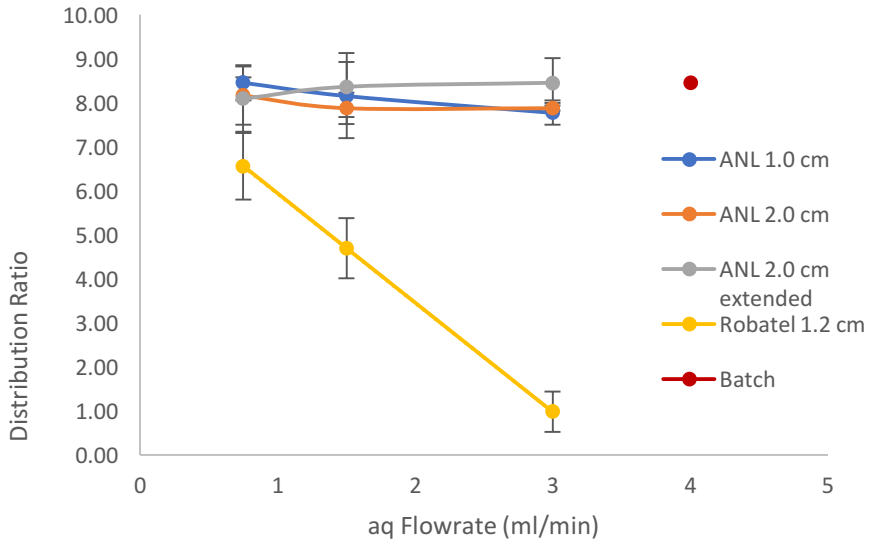

Figure 27. Distribution ratios of dysprosium as a function of flowrate. Aqueous phase was 0.1 mM $Dy(NO_3)_3$ in 0.1 M NO_3 and the organic phased was 0.2 M C572, org:aq flow rate ration was at 1:1. Distribution ratio for batch extraction is showed for comparison.

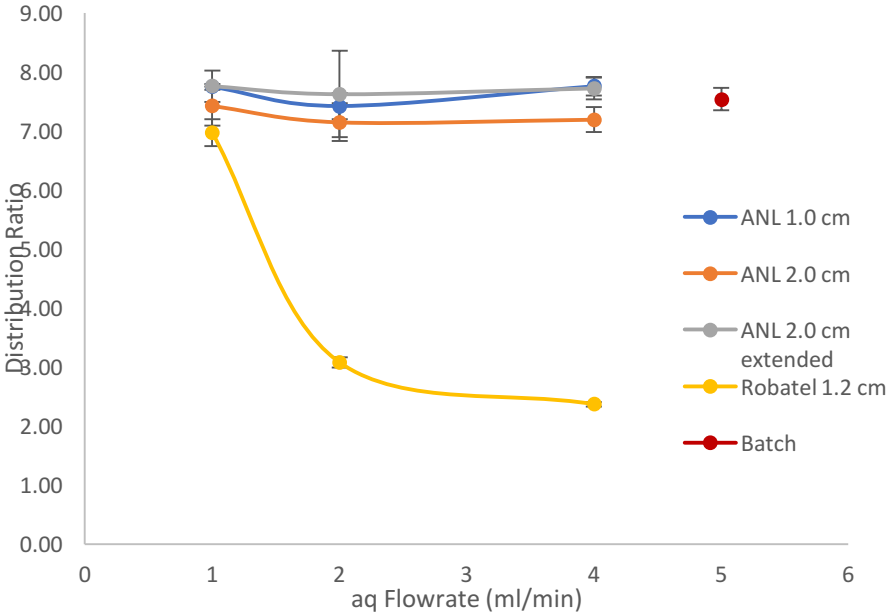

Figure 28. Distribution ratios of dysprosium as a function of flowrate. Aqueous phase was 0.1 mM $Dy(NO_3)_3$ in 0.1 M NO_3 and the organic phased was 0.2 M C572, org:aq flow rate ration was at 2:1. Distribution ratio for batch extraction is showed for comparison.

As it is apparent from the graphs, at both flow rate ratios the Robatel contactor has a much lower efficiency compared to the ANL contactors especially at higher flowrates. It is however worth noting that the Robatel had yielded distribution ratios close to 7 using the same extraction system in earlier studies at total flowrates of 3 and 6 ml/min. Therefore, the huge drop in the D value in

this study could either be due to concentration mismatches, which is unlikely to have been so great, or because the Robatel is hydrodynamically unstable. For example, syphoning was frequently observed during experiments with the Robatel contactor. The very rapid kinetics of extraction of this system is perhaps the reason why all three ANL contactors have yielded very close values. To better assess the extent of the effectiveness of the extended mixing zone in one of the 2 cm contactors a system with slower extraction kinetics should be tested.

Additional comparisons between the contactors were carried out using a system of uranyl extraction by TBP in n-dodecane. The aqueous phase consisted of 10 mM uranyl nitrate in 3.5 M HNO_3 and the organic system of 1 M TBP in dodecane. After both phases started exiting the contactor, the time was started and samples from both phases were collected over time to also check for the stability of operations. The results are shown in Figures 29 and 30. Experiments were conducted under two conditions. Aqueous to organic flowrate ratio of two and three. The organic flowrate was fixed at 1 ml/min and the aqueous one was set accordingly.

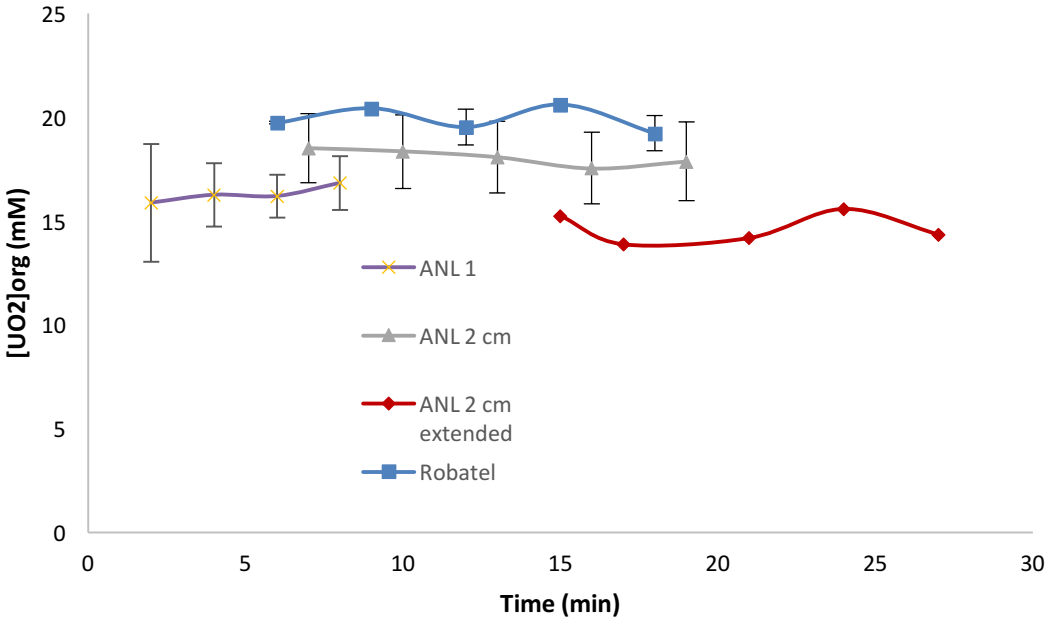

Figure 29. Extraction of uranyl nitrate by 1 M TBP in dodecane at organic flowrate of 1 ml/min and aqueous flowrate of 2 ml/min.

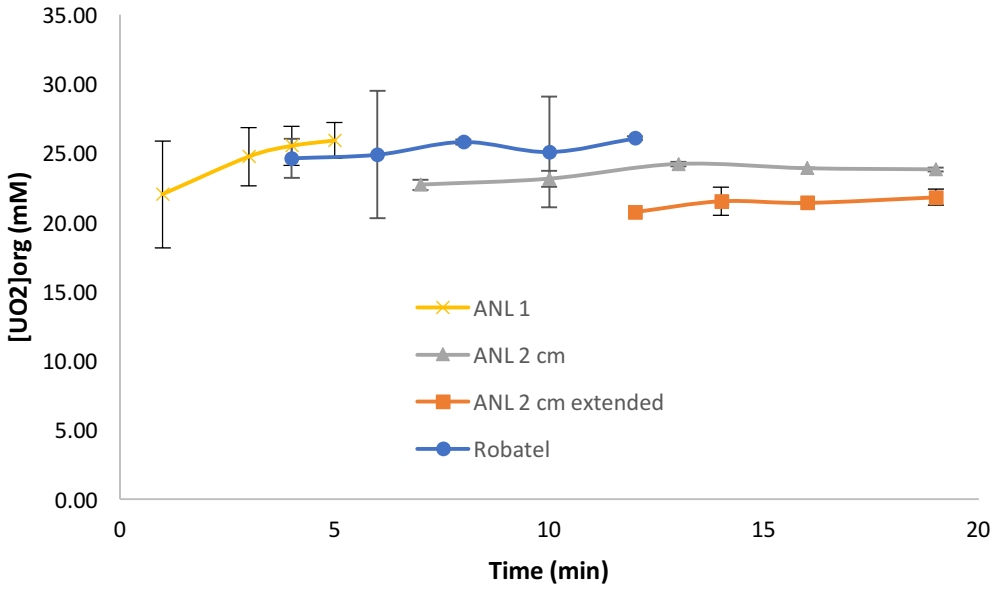

Figure 30. Extraction of uranyl nitrate by 1 M TBP in dodecane at organic flowrate of 1 ml/min and aqueous flowrate of 3 ml/min.

This extraction system provided more comparable values between the different contactors. It is worth noting that the ANL contactor with extended mixing zone has the lowest efficiency among the four contactors. After collecting the samples, both pumps were stopped, and the content of the mixing zone was drained into a graduated cylinder. Then, the rotor was stopped, and its content collected into a separate graduated cylinder. Samples were collected from both phases to check for the concentration of uranium in the mixing and separating zones. It was noticed that in some cases the extraction progressed during the separation step as the mixing zone had lower distribution values compared to the ones from the separation zone, which match the distribution ratios from the exits.

In addition to performance testing, residence time distribution analysis was performed on the 2 cm ANL contactor. As opposed to the Robatel contactor, the 2.0 cm ANL contactors have a valve allowing to drain the content of the contactor for physical measurements. At the end of the RTD experiments, the pumps were stopped and the mixing zone was immediately drained. After this, the rotor was stopped to drain its content. This allowed us to get an estimate of the volume ratio between the mixing zone and the settling zone.

The results from the RTD experiments are shown in Figures 31 and 32. It can be seen that the concentration of the injected pulse in the outlet stream has still not reached zero even after an extended time. In the case of 4 ml/min aqueous flow rate, the experiment was repeated several times in an attempt to reach the point when all tracer had left the contactor but all attempts were unsuccessful. As Figure 33 shows, even when the concentration is slightly above zero, the plot of the first moment of the RTD probability function remains quite high giving incorrect information about the average residence time. This may be due to dormant regions in the contactors that take a while to flush out after the injected pulse.

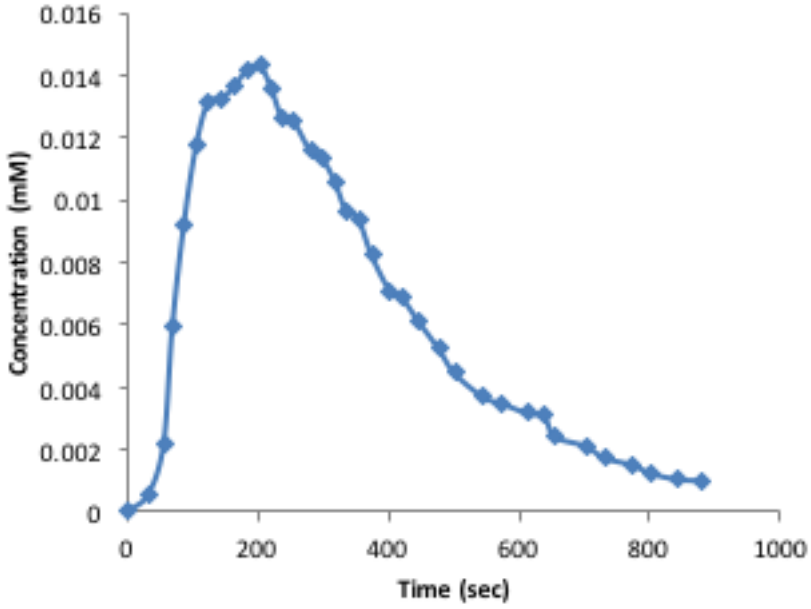

Figure 31. Concentration of tracer $Dy(NO_3)_3$ in the outlet aqueous stream as a function of time in the ANL 2.0 cm centrifugal contactor at flowrate 2 ml/min aqueous and ratio of 2/1.

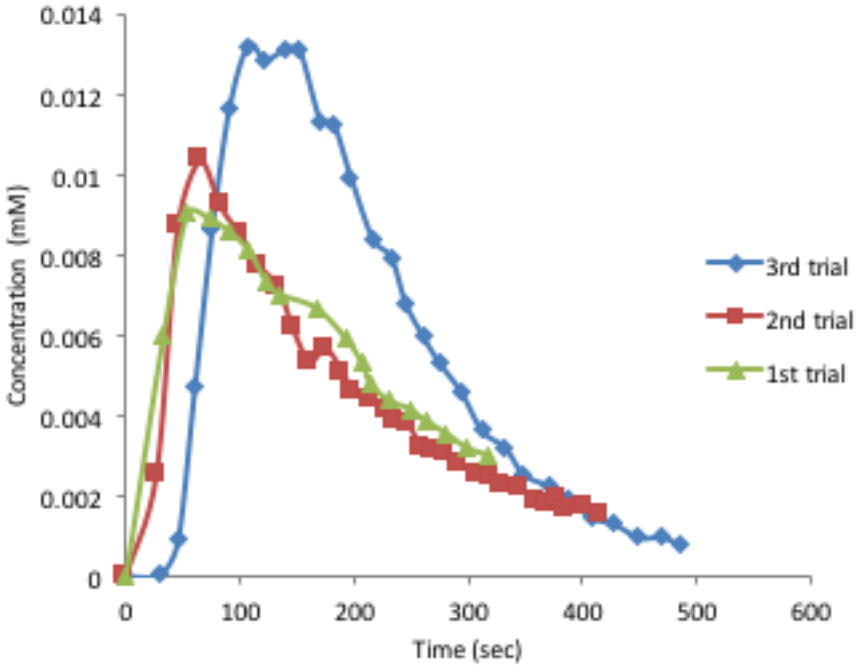

Figure 32. Concentration of tracer $Dy(NO_3)_3$ in the outlet aqueous stream as a function of time in the ANL 2.0 cm centrifugal contactor at flowrate 4 ml/min aqueous and ratio of 2/1.

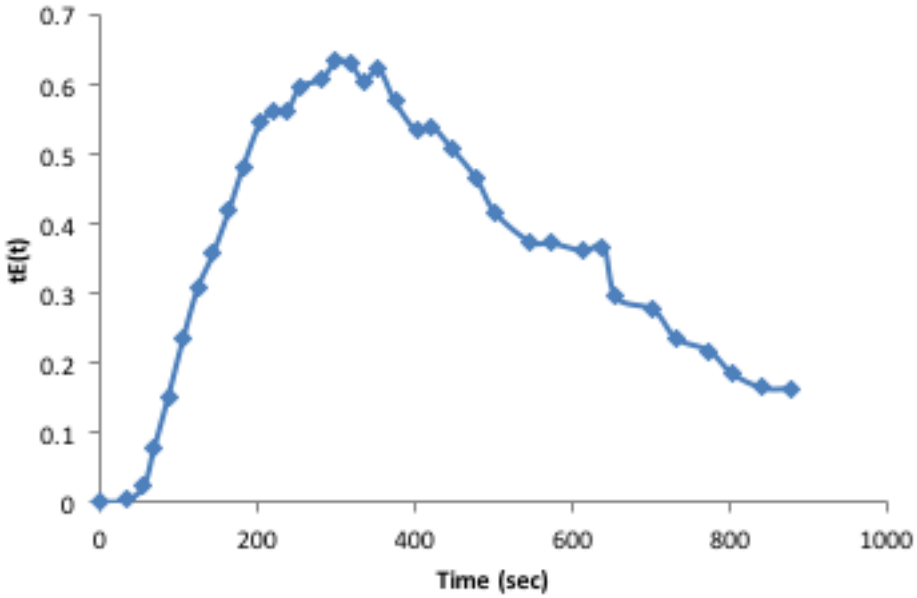

Figure 33. First moment of the residence time probability function as a function of time in the ANL 2.0 cm centrifugal contactor at flowrate 2 ml/min aqueous and ratio of 2/1.

Overall, it was found that the 3D printed contactors performed superior compared to the Robatel contactor. Additional experiments are required to characterize the hydrodynamics of these contactors.

3.3. Extraction kinetic studies

One of the key values that is required for validating the CFD simulations when mass transfer is added, as well as for estimating the interfacial area between the aqueous and organic phase in the contactor mixing zone, is the mass transfer coefficient. In order to find values for this we carried out a number of studies using stirred cells. Our first sets of kinetic data were collected using a Lewis cell. However, it was found that this setup was not useful for determining the mass transfer coefficient of dysprosium into an organic phase by extraction with Cyanex 572. The stirring of each phase in the Lewis cell was not sufficient to reach the conditions where the extraction was limited by the reaction rate and we were most likely operating in a mixed regime where diffusion cannot be discounted as a rate limiting step.

To reduce the effect of slow diffusion a Nitsch cell was constructed and installed, see Figure 34 below. The design was based on drawings supplied to us from a group in FZK in Germany, colleagues of our international collaborator. In the fabrication and setup of this experimental rig we encountered numerous challenges in terms of material degradation in the o-rings and bearings, fluctuations in the RMP in the initial stirrer motors used, etc. All the issues were corrected and the instrument is working satisfactory. However, at the end of this project we had only limited amount of time to collect high quality data.

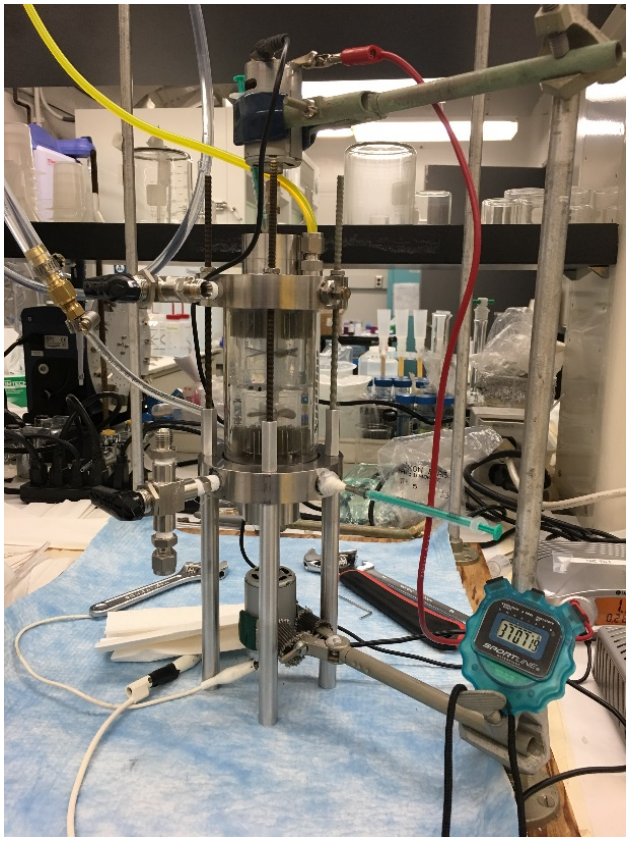

Figure 34. Nitsch Cell for extraction kinetics studies.

Some of the data collected using the Nitsch cell is shown below in Figure 35. In this study, the organic phase stirrer speed was fixed at 400 RPM, which is the maximum achievable prior to breaking the otherwise laminar interphase, and the aqueous phase stirrer speed was incrementally increased to note the increase in the observed rate constant as the stagnant diffusion layer becomes thinner. However, a plateau region where the process would be chemically driven away from diffusion effects could not be achieved before breaking the interface.

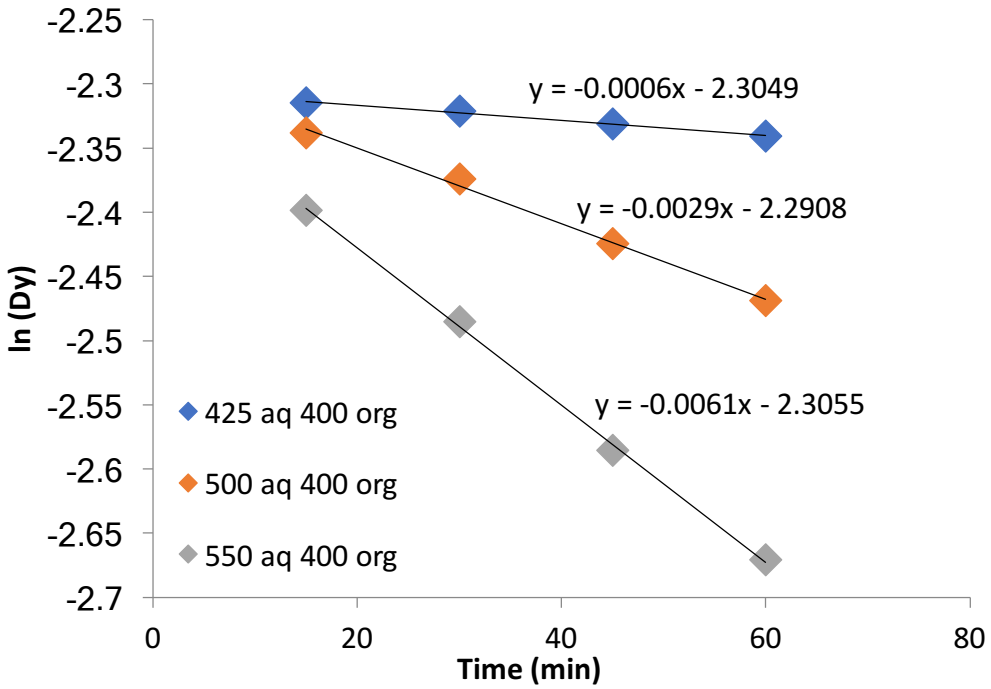

Figure 35. The slopes of the lines represent the observed initial rate constants in the extraction of 0.1 mM $Dy(NO_3)_3$ in 0.1 M HNO_3 & 0.2 M C572 in IsoparL at 400 RPM org stirring and 25.0 C

In order to slow down the true kinetics of the system, we lowered the temperature to 10 °C. Looking at Figure 36, it is evident that past 300 RPM a plateau region was finally achieved.

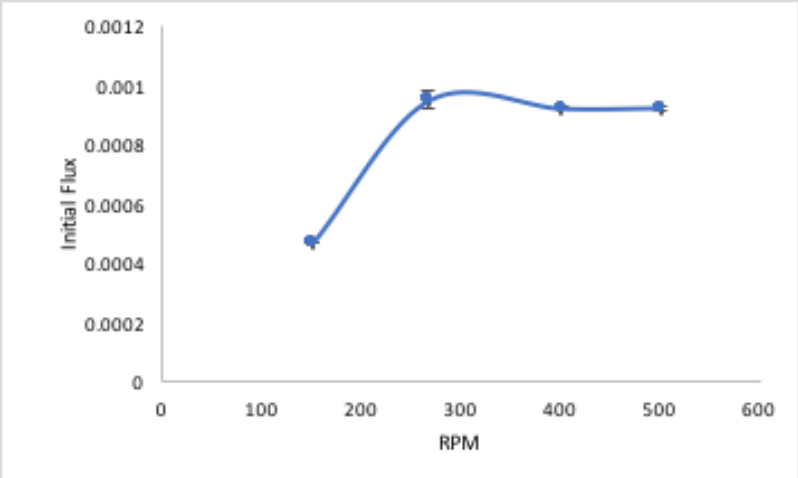

Figure 36. Initial flux values of the extraction of 0.1 mM $Dy(NO_3)_3$ in 0.1 M HNO_3 with 0.2 M C572 in Isopar L at 10.0 C.

Collecting kinetic data at various temperatures would allow us to extrapolate the kinetics of mass transfer to conditions relevant for the centrifugal contactors and fully evaluate the hydrodynamics. This work in underway and will be disseminated in peer reviewed journals crediting this project.

4. CFD calculations on annular centrifugal contactors

To understand the hydrodynamics of the flow in the contactor, computational fluid dynamics (CFD) was applied to simulate the flow. The CFD calculations were initially carried out under the direction of Dr. Kent Wardle at ANL and were later under the direction of Dr. Nathaniel Hoyt as Dr. Wardle left ANL and the project. For these calculations, we had access to computer resources at INL through our collaborator there (Dr. Zalupski).

OpenFOAM, an open source software based on the finite volume method, was used to create the simulations. Some preliminary simulations, Figures 37 and 38, with simplified contactor geometries were obtained. The residence time distribution experiments described above were designed to validate the outcomes of these simulations.

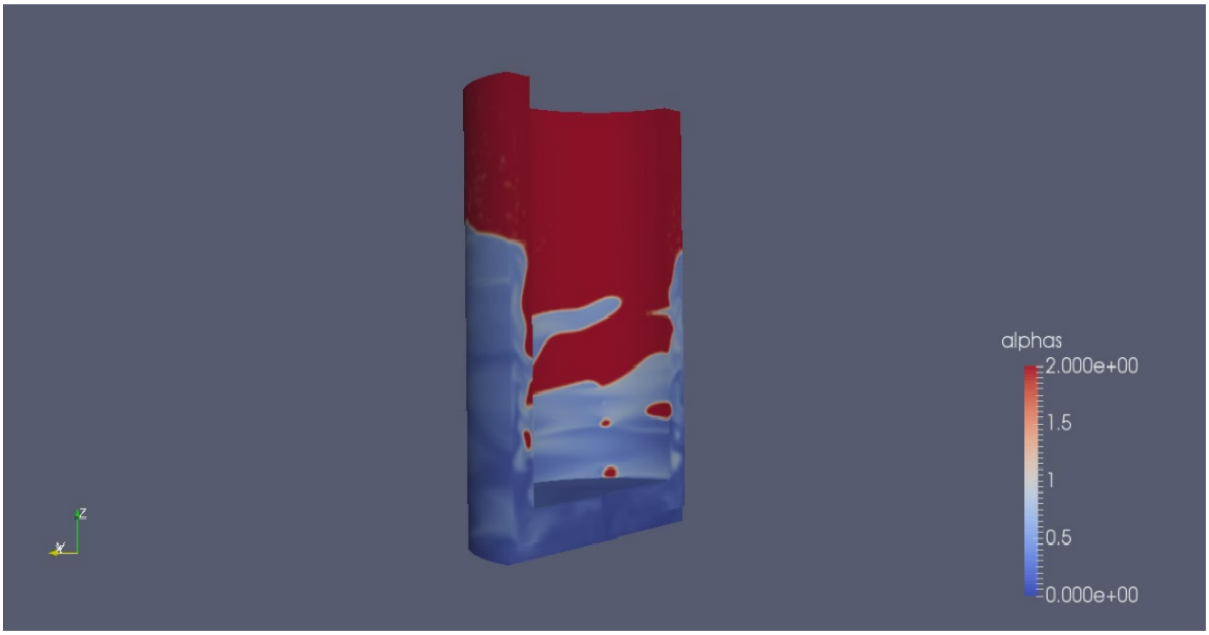

Figure 37. Multiphase flow in the mixing zone of the Robatel BXP12 with straight vanes at the bottom of the contactor. The red color is air, the gray color is oil, and the blue color is water.

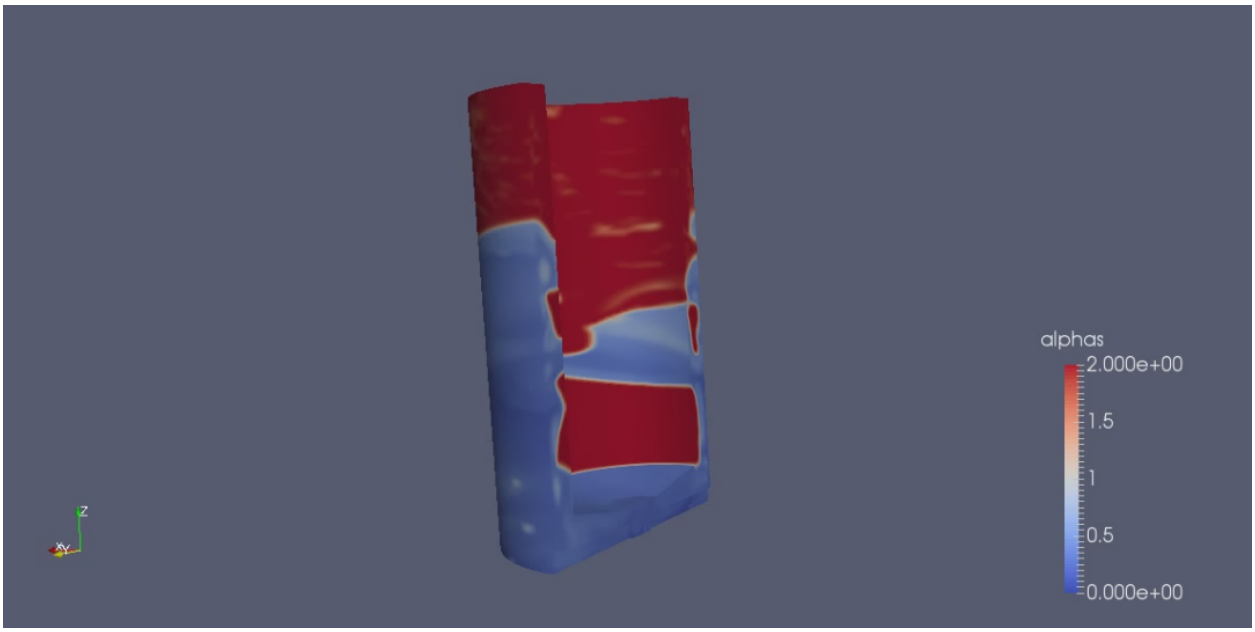

Figure 38. Multiphase flow in the mixing zone of the Robatel BXP12 with straight vanes at the bottom of the contactor and allowing the fluid to exit the mixing zone through a gap at the bottom of the rotor. The red color is air, the gray color is oil, and the blue color is water.

In order to utilize CFD simulations to predict extraction efficiency significant effort was invested to improve the CFD solver. The main addition was the mass transfer capability which is required for full extraction simulations. The solver performs mass transport calculations for an arbitrary number of disperse chemical species and has terms to account for transfer of the species from one phase to another (i.e., from the aqueous phase to the organic phase for extraction). For these simulations to be meaningful the mass transfer kinetic coefficient must be known, which is why we carried out the stirred cell studied described above.

A lot of work "under the hood" was done to make the solver run stably for long simulations (numerical issues with the previous solver had a tendency to cause crashes every few hours - which is not ideal for simulations that can require a couple of weeks to run).

Previously existing solver features:

- Multiple phases (aqueous, organic, air)
- Turbulence (LES)
- Coupled hybrid multiphase treatment (dispersed/segregated)
- Rotating volumes

New solver features:

- Mass Transfer of Dispersed Species
- Convection-diffusion mass transfer to interface from disperse phase
- Kinetics of forward and back-extraction at interface
- Convection-diffusion mass transfer to interface from continuous phase
- Solver stabilization

With these improvements in the software our intent was to validate the simulations using experimental data from both the 5 cm CINC contactor as well as the Robatel BXP12 contactor. Due to delays in getting accurate mass transfer kinetic data our simulations were held up. We intend on validating the improved code with a relatively simple system and these validations are underway and will be disseminated in a future journal publication, crediting this project.

Objective 3. Provide a theoretical/simulation and experimental base for scale-up of batch-wise extraction to continuous contactors.

In this third objective, we planned to show a connection between experimental results on extraction, molecular dynamic simulations and computational fluid dynamics and to provide some guidelines on scaling up to multiple contactors. The connection between experiments, MD and CFD is the mass transfer coefficient. This value can be determined experimentally via stirred cell experiments. This value can also be determined by MD simulations of the energy of mass transfer of the extracted complex. This value will then be provided to the CFD solver to predict the performance of a centrifugal contactor, which will be further validated by experimental results. Of course, the mass transfer coefficients are dependent on the conditions associated with the flow surrounding the aqueous/organic interface and care must be taken when comparing different values.

During this 3-year project we were not able to reach this goal of providing the connection between these methods. Significant improvements were made in the simulations and significant challenges were faced and overcome on the experimental side giving us confidence that it should be possible to show this connection and we will attempt to finalize any studies that were initiated during this project and present the results in future journal articles and conference presentations.

References:

(1) Wang, J.; Wolf, R. M.; Caldwell, J. W.; Kollman, P. A.; Case, D. A. Development and Testing of a General Amber Force Field. *J. Comput. Chem.* **2004**, *25* (9), 1157–1174.

(2) Grossfield, A. *WHAM: the Weighted Histogram Analysis Method, Version 2.0.9*; http://membrane. urmc. rochester. edu/content/wham, 2012.

(3) Petković, D. M. Some Correlations of Trialkyl Phosphates Dimerization Constants. *J. Inorg. Nucl. Chem.* **1968**, *30* (2), 603–609.

(4) Dyrssen, D.; Petković, D. Distribution Studies of Tripropyl Phosphate Between Different Organic Diluents and Water. *J. Inorg. Nucl. Chem.* **1965**, *27* (6), 1381–1393.

(5) Janini, G.M.; Katrib, A.H. Determination of the dipole moment of polar compounds in nonpolar solvents, *J. Chem. Edu.* **1983**, 60 (12), 1087.

(6) Luo, J.; Wang, C.-Z.; Lan, J.-H.; Wu, Q.-Y.; Zhao, Y.-L.; Chai, Z.-F.; Niec, C.-M.; Shi, W.-Q. Theoretical studies on the AnO_2^{n+} (An = U, Np; n = 1, 2) complexes with di-(2-ethylhexyl)phosphoric acid, *Dalton Trans.* **2015**, *44*, 3227-3236.

Conclusions for the project and Future work

Based on observations made in this project it is possible that using well validated simulations one can predict and inform experimental studies. We saw this directly in the trimers of TBP that first were observed in simulation and verified experimentally. The computational tools for molecular dynamics at hand are undoubtedly powerful and a wealth of information can be gained. However, care should be taken to ensure that simulations are carried out for a long enough period of time to reach an equilibrium. Furthermore, the expensive simulations using polarizable force fields may still yield unreasonable results depending on the starting conditions. CFD simulations are useful for describing the fluid mechanics while the mass transfer simulations are yet to be validated.

To successfully provide a connection between the different simulation scales and experimental work considerable amount of carefully collected data is needed, requiring stable experimental setups and procedures.

Work initiated during this project that we intend to bring to fruition within the year following the end of this project include: phase transfer kinetic studies; validation of the mass transfer solver in OpenFOAM; simulation of the hydrodynamics in a miniature centrifugal contactor; and simulation of the extraction of uranyl nitrate in a stirred cell.

Publications and presentations.

During this project, we have published 4 peer reviewed journal papers (P1-P4), with one additional paper just accepted with minor revisions (P5). Furthermore, 3 peer reviewed conference proceedings (CP1-CP3) based on the work carried out here has been published.

P1. Vo, Q., Hawkins, C., Dang, L., Nilsson, M., Nguyen, H. A Computational Study of Molecular Structure and Self-Association of Tri-n-butyl Phosphates in n-Dodecane Diluent. *J. Phys. Chem. B, 119*(4), 1588-15897, **2015**. doi: 10.1021/jp510365c

P2. Vo, Q., Dang, L., Nilsson, M., Nguyen, H. D. Quantifying Dimer and Trimer Formation by Tri-N-Butyl Phosphates in N-Dodecane: Molecular Dynamics Simulations. *J. Phys. Chem. B, 120*(28), 6985–6994, **2016**. doi: 10.1021/acs.jpcb.6b02924

P3. Vo, Q., Unangst, J., Nguyen, H. D., Nilsson, M. Quantifying Dimer and Trimer Formation by Tri-N-Butyl Phosphates in N-Dodecane: FTIR Study. *J. Phys. Chem. B, 120*(28), 6976–6984, **2016**. doi: 10.1021/acs.jpcb.6b02923

P4. Dang, L. X., Vo, Q. N., Nilsson, M., Nguyen, H. D. Rate theory on water exchange in aqueous uranyl ion. *Chem. Phys. Letters, 671*, 58-62, **2017**. doi: http://dx.doi.org/10.1016/j.cplett.2017.01.020

P5. Yoo, T., Nguyen, H., Nilsson, M. Determinations of Dipole Moments for Liquid-Liquid Extraction Reagents. Journal of Solution Chemistry, Accepted with minor revisions, **2018**.

CP1. Vo, Q., Nilsson, M., Nguyen, H. D. Computational Study of Self-Association of Tri-n-butyl Phosphate in n-Dodecane. In, Transactions of the American Nuclear Society. The American Nuclear Society, **2015**.

CP2. Vo, Q., Nilsson, M., Nguyen, H. D. Molecular Dynamics Simulations and Experimental Studies of Tri-n-butyl Phosphate for Liquid-Liquid Extraction [Conference]. In, Nuclear Fuel Cycle For a Low-Carbon Future. GLOBAL-2015: International Nuclear Fuel Cycle Conference. Paris, France, **2015.**

CP3. Babikian, T., Nilsson, M. Extraction Kinetics and Hydrodynamics in Miniature Annular Centrifugal Contactors. In, Nuclear Energy Innovation to the Carbon-Free World. GLOBAL-2017: International Nuclear Fuel Cycle Conference. Seoul, Korea, **2017.**

In addition to these publications the data collected is currently being compiled in at least 4 additional publications for peer reviewed journals.

The work has been presented at a number of international and domestic conferences as well as invited seminars at various educational and research institutions. In total 8 oral presentations and 8 poster presentations have been given by the PIs or students from the project. Below is a list of all the presentations in reverse chronological order, the presenter is underlined.

11/6/2017	"Quantifying TBP dimers and trimers in alkane solutions via Simulations and Experiments", ISEC' 2017, Miyazaki, Japan, Oral Presentation, Vo, Q., Unangst, J., Nguyen, H., Dang, L., Nilsson, M.
09/27/2017	"Extraction Kinetics and Hydrodynamics in Miniature Annular Centrifugal Contactors", Global 2017: International Nuclear Fuel Cycle Conference, Seoul, South Korea, Poster Presentation, Babikian, T., Nilsson, M.
05/23/2017	"A Kinetic and Hydrodynamic Study of the Robatel BXP012 Annular Centrifugal Contactor", 41st Annual Actinide Separations Meeting, Argonne National Lab, IL, USA, Poster Presentation, Babikian, T., Nilsson, M.
03/07/2017	"Quantifying TBP dimers and trimers in alkane solutions via Simulations and Experiments", 2017 Waste Management Symposia, Phoenix, AZ, USA, Poster Presentation, Vo, Q., Dang, L., Nguyen, H., Nilsson, M.
11/15/2016	"Extraction Kinetics and Hydrodynamics in Miniature Annular Centrifugal Contactors", 2016 AIChE Annual Meeting, American Institute of Chemical Engineers, San Francisco, USA, Oral Presentation, Babikian, T., Nilsson, M.
10/12/2016	"Combining Experiments and Simulations in Separation Processes for Used Nuclear Fuel", 19th Symposium on Separation Science and Technology, Gatlinburg, TN, USA, Oral Presentation, Nilsson, M., Babikian, T., Vo, Q., Yoo, T., Dang, L., Nguyen, H., Wardle, K., Hoyt, N.
10/12/2016	"Extraction Kinetics and Hydrodynamics in Miniature Annular Centrifugal Contactors", 19th Symposium on Separation Science and Technology, Gatlinburg, TN, USA, Oral Presentation, Babikian, T., Nilsson, M.

08/31/2016	"Quantifying TBP dimers and trimers in alkane solutions via simulations and experiments", 9th International Conference on Nuclear and Radiochemistry - NRC9, Helsinki, Finland, Poster Presentation, Vo, Q., Unangst, J., Dang, L., Nguyen, H., Nilsson, M.
05/24/2016	"Extraction Kinetics and Hydrodynamics in Miniature Annular Centrifugal Contactors", 40th Annual Actinide Separations Meeting, Del Mar, CA, USA, Poster Presentation, Babikian, T., Nilsson, M.
05/24/2016	"Quantifying TBP dimers and trimers in alkane solutions via MD Simulations and Experiments", 40th Annual Actinide Separations Meeting, Del Mar, CA, USA, Poster Presentation, Vo, Q., Unangst, J., Dang, L., Nguyen, H., Nilsson, M.
09/24/2015	"Molecular Dynamics Simulations and Experimental Studies of Tri-n-butyl Phosphate for Liquid-Liquid Extraction", Global 2015: International Nuclear Fuel Cycle Conference, Paris, France, Oral Presentation, Vo, Q. Nilsson, M., Nguyen, H.
06/08.2015	"Computational Study of Self-Association of Tri-n-butyl Phosphate in n-Dodecane", American Nuclear Society Annual Meeting, San Antonio, TX, USA, Oral Presentation, Vo, Q., Nguyen, H., Nilsson, M.
05/20/2015	"Computational Study of Self-Association of Tri-n-butyl Phosphate in n-Dodecane", 39th Annual Actinide Separations Meeting, Salt Lake City, UT, USA, Poster Presentation, Vo, Q., Nguyen, H., Nilsson, M.
05/20/2015	"Extraction Kinetics of Dysprosium in Annular Centrifugal Contactors", 39th Annual Actinide Separations Meeting, Salt Lake City, UT, USA, Poster Presentation, Babikian, T., Nilsson, M.
04/16/2015	"Molecular Dynamics Simulations and Experimental Studies of Tri-n-butyl Phosphate for Liquid-Liquid Extraction", MARC X: Tenth International Conference on Methods and Applications of Radioanalytical Chemistry, Kona, HI, USA, Oral Presentation, Vo, Q., Nilsson, M., Nguyen, H.
11/18/2014	"A Computational Study of Molecular Structure and the Self-Association of Tri-n-butyl Phosphate in n-Dodecane Diluent", 2014 AIChE Annual Meeting, American Institute of Chemical Engineering, Atlanta, GA, USA, Oral Presentation, Vo, Q., Hawkins, C., Dang, L., Nguyen, H., Nilsson, M.

Outcomes and markers of success

As this was a project led from a university one of most important products was the education and training of students. Over the course of this project 4 graduate students (Quynh Vo, Ted Yoo, Tro Babikian and Alba Font Bosch) and 3 undergraduate students (Alex Afesi, Kevin Tlaxcalteca and Ever Velasquez) were directly involved in the work. All undergraduate students have graduated and found jobs in industry or continued to graduate school. One of the graduate students, Quynh Vo, is scheduled to graduate in March 2018. Two of the other graduate students (Tro and Ted) passed their qualifying exam during the course of this project and will graduate in the 2018-2019 academic year. Alba will graduate with a MS degree in the beginning of 2018. The graduate students were given chances to visit the national labs. Quynh visited PNNL on several occasions and worked with Dr. Liem while staying there. Tro visited ANL worked with Dr. Holt. These visits not only helped the students in their research projects but also helped build important connections for their future careers.

Finally, this project resulted, so far, in 8 publications and 18 presentations with more publications underway. In all the publications and presentations, we acknowledged the funding source for this work.